

Continuous Diffusion Model for Language Modeling

Jaehyeong Jo¹ Sung Ju Hwang^{1,2}

Abstract

Diffusion models have emerged as a promising alternative to autoregressive models in modeling discrete categorical data. Yet diffusion models that directly work on discrete data space do not fully exploit the power of iterative refinement, as the signals are lost during the transition between discrete states. Existing continuous diffusion models for discrete data have limited performance compared to discrete approaches, and the unclear link between them restricts the development of diffusion models for discrete data. In this work, we propose a continuous diffusion model for language modeling that incorporates the geometry of the underlying categorical distribution. We establish a connection between the discrete diffusion and continuous flow on the statistical manifold, and building on the analogy, we introduce a simple design for the diffusion process that generalizes previous discrete diffusion models. We further propose a simulation-free training framework based on radial symmetry and a simple technique to address the high dimensionality of the manifold. Comprehensive experiments on language modeling benchmarks and other modalities show that our method outperforms existing discrete diffusion models and approaches the performance of autoregressive models. Codes available at <https://github.com/harryjo97/RDLM>.

1. Introduction

Discrete diffusion models (Austin et al., 2021; Lou et al., 2024) emerged as a promising competitor to autoregressive models for the generative modeling of discrete data. These models have demonstrated competitive performance on tasks such as language modeling (Shi et al., 2024; Sahoo et al., 2024) and code generation (Gat et al., 2024). Unlike

autoregressive models that generate data sequentially, diffusion models generate the sequence in parallel, allowing for bidirectional controllable generation and faster sampling.

However, discrete diffusion models do not fully leverage the power of iterative refinement which is the key to generative modeling of continuous data, for example, image synthesis (Saharia et al., 2022; Esser et al., 2024) and video generation (Polyak et al., 2024; Brooks et al., 2024). In discrete diffusion models, the progressive corruption during the forward process is modeled by stochastic jumps between states in Markov chains. Since denoising is achieved by jumping between states, discrete diffusion loses valuable signals during refinement which limits the generative performance and controllability.

Several efforts were made to adapt continuous diffusion models for discrete data, but their performance falls short of discrete diffusion models, demonstrating a significant gap compared to autoregressive models. Past works applied diffusion models for images to discrete data through continuous relaxation without constraint (Han et al., 2022; Li et al., 2022). Other lines of works (Avdeyev et al., 2023; Stärk et al., 2024) map discrete data to the probability simplex which exerts a strong prior assumption on Dirichlet distribution, but often fails to model complex patterns. This led to recent works (Cheng et al., 2024; Davis et al., 2024) that apply flow matching to learn the categorical distributions using the structure of the statistical manifold, but these methods are limited to small sequences and categories. In particular, the link between discrete and continuous diffusion remains unclear, hindering the development of a coherent diffusion framework for discrete data.

In this work, we present Riemannian Diffusion Language Model (RDLM), a continuous diffusion framework for language modeling that incorporates the geometry of the statistical manifold in the diffusion processes. We establish a connection between continuous flow on the statistical manifold and the discrete diffusion process, showing that the trajectory of the transition distribution can be modeled to a conditional flow on the manifold. Based on the analogy, we introduce a simple design of the diffusion processes on the manifold that generalizes previous discrete diffusion models. We further present a simulation-free training scheme using radial symmetry that integrates simple parameterization and

¹Korea Advanced Institute of Science and Technology (KAIST) ²DeepAuto.ai. Correspondence to: Jaehyeong Jo <harryjo97@kaist.ac.kr>, Sung Ju Hwang <sungju.hwang@kaist.ac.kr>.

maximum likelihood-based training objectives. Through experiments on language modeling tasks, image modeling, and biological sequence design, we validate that our framework outperforms existing discrete diffusion models.

2. Background

2.1. Discrete diffusion models

Discrete diffusion models (Austin et al., 2021; Lou et al., 2024; Sahoo et al., 2024; Shi et al., 2024) define the diffusion process directly on discrete structures using the Markov chains. The forward process describes the transition from the current state to other states, which is formalized by multiplying the transition matrix Q_t :

$$q(x_t|x_{t-1}) = \text{Cat}(x_t; Q_t x_{t-1}), \quad (1)$$

where x_t is the random variable for the discrete states and $\text{Cat}(\cdot)$ denotes the categorical distribution. This induces the marginal distribution that corresponds to repeatedly multiplying the transition matrices over time steps:

$$q(x_t|x) = \text{Cat}(x_t; \bar{Q}_t x) = \text{Cat}(x_t; Q_t \cdots Q_1 x). \quad (2)$$

Austin et al. (2021) introduced several designs of the transition matrices, including the masked (absorbing state) diffusion and the uniform diffusion, and the continuous-time Markov chains (CTMC) (Austin et al., 2021; Campbell et al., 2022) extends the framework to continuous-time.

2.2. Statistical Manifold of Categorical Distribution

Let $\mathcal{X} = \{1, \dots, d\}$ denote the discrete data space and $\Delta^{d-1} = \{(p_1, \dots, p_d) \in \mathbb{R}^d | \sum_i p_i = 1, p_i \geq 0\}$ denote the $(d-1)$ -dimensional probability simplex. A d -class categorical distribution over \mathcal{X} can be parameterized by the parameters p_1, \dots, p_d such that $\{\sum_i p_i = 1, p_i \geq 0\}$. Then the statistical manifold $\mathcal{P}(\mathcal{X})$ of the categorical distribution corresponds to Δ^{d-1} equipped with the Fisher-Rao metric (Rao, 1992; Amari, 2016) (see Appendix A.1). Moreover, there exists a diffeomorphism from $\mathcal{P}(\mathcal{X})$ to the positive orthant of a $(d-1)$ -dimensional sphere \mathbb{S}_+^{d-1} :

$$\pi : \mathcal{P}(\mathcal{X}) \rightarrow \mathbb{S}_+^{d-1}; p_i \mapsto u_i = \sqrt{p_i}, \quad (3)$$

which induces the following geodesic distance on \mathbb{S}_+^{d-1} :

$$d_g(\mathbf{u}, \mathbf{v}) = \cos^{-1} \langle \mathbf{u}, \mathbf{v} \rangle, \quad (4)$$

where $\langle \cdot \rangle$ denotes the Euclidean inner product. We provide further explanation in Appendix A.1.

2.3. Riemannian Diffusion Mixture

Riemannian diffusion mixture framework (Jo & Hwang, 2024) provides a simple approach to generative modeling

on general manifolds. The construction of the generative model starts with defining a bridge process \mathbb{Q}^z on the manifold \mathcal{M} with endpoint z : $d\mathbf{X}_t^z = \eta^z(\mathbf{X}_t^z, t)dt + \sigma_t dB_t^{\mathcal{M}}$ where $B_t^{\mathcal{M}}$ is the Brownian motion defined on \mathcal{M} . The diffusion process transporting an initial distribution to the data distribution is modeled as a mixture of bridge processes:

$$d\mathbf{X}_t = \left[\int \eta^z(\mathbf{X}_t, t) \frac{p_t^z(\mathbf{X}_t)}{p_t(\mathbf{X}_t)} p^*(d\text{vol}_z) \right] dt + \sigma_t dB_t^{\mathcal{M}} \quad (5)$$

where p^* denotes the data distribution, p_t^z is the marginal distribution of the bridge \mathbb{Q}^z , and $p_t(\cdot) := \int p_t^z(\cdot) p^*(d\text{vol}_z)$. The drift of this process is regressed by a neural network η^θ with the bridge matching objective:

$$\mathbb{E}_{\substack{\mathbf{z} \sim p^* \\ \mathbf{X} \sim \mathbb{Q}^z}} \left[\int_0^T \left\| \sigma_t^{-1} \left(\eta^\theta(\mathbf{X}_t, t) - \eta^z(\mathbf{X}_t, t) \right) \right\|_{\mathcal{M}}^2 dt \right] \quad (6)$$

We provide further details in Appendix A.4.

3. Riemannian Diffusion Language Model

We introduce a novel continuous diffusion model for language modeling. In this section, we first present a single token generation framework, which we generalize to modeling sequences of tokens in Section 5.

3.1. Generalization of Discrete Diffusion

Continuous Reparameterization of Discrete Data To incorporate the geometry of the underlying categorical distribution, we leverage the statistical manifold to parameterize discrete data (Cheng et al., 2024; Davis et al., 2024). Each point on the statistical manifold $\mathcal{P}(\mathcal{X})$ corresponds to the parameters of a categorical distribution over the discrete sample space $\mathcal{X} = \{1, \dots, d\}$. Thus discrete data can be represented as continuous parameters of categorical distribution on the manifold.

Yet the Fisher-Rao metric is ill-defined on the boundary of the manifold where the initial distribution of the parameterized data lies, incurring numerical issues near the boundary. To address this, we leverage the diffeomorphism π (Eq. (3)) which maps $\mathcal{P}(\mathcal{X})$ to the positive orthant of a hypersphere \mathbb{S}_+^{d-1} (Cheng et al., 2024; Davis et al., 2024), where $\mathbf{u} \in \mathbb{S}_+^{d-1}$ corresponds to $\text{Cat}(\cdot; \pi^{-1}(\mathbf{u}))$. Therefore, discrete data can be reparameterized to continuous states on \mathbb{S}_+^{d-1} while preserving the geometry of the categorical distribution. In the case of masked diffusion, discrete sample space is augmented with an additional mask state, and the reparameterization results in a d -dimensional sphere.

Our key observation is that the transition distribution $q_t(x_t|x_0)$ of a discrete diffusion process is a categorical distribution on \mathcal{X} (Eq. (2)). Therefore, modeling q_t is equivalent to modeling the probability path on the statistical manifold $\mathcal{P}(\mathcal{X})$. From the following proposition, we show that

discrete diffusion models over \mathcal{X} can be modeled by a continuous flow on $\mathcal{P}(\mathcal{X})$ and further on \mathbb{S}_+^{d-1} (we defer the proof to Appendix A.2).

Proposition 3.1. *The transition distribution of discrete diffusion processes can be modeled by the probability path on the statistical manifold, and further on the hypersphere.*

proof sketch. A continuous flow on \mathbb{S}_+^{d-1} that interpolates \mathbf{v} and \mathbf{u} as geodesic is described by the following ODE:

$$\frac{d\mathbf{Y}_t}{dt} = -\frac{d \log \kappa_t}{dt} \exp_{\mathbf{Y}_t}^{-1}(\mathbf{u}), \quad \mathbf{Y}_0 = \mathbf{v}, \quad (7)$$

where \exp_x^{-1} denotes the logarithm map. Then for well-designed schedule κ_t and \mathbf{u} , the process $\mathbf{Z}_t := \pi(\mathbf{Y}_t)$ on $\mathcal{P}(\mathcal{X})$ corresponds to the transition distribution of the discrete diffusion process. In particular, we obtain the masked diffusion process for $\mathbf{u} = \mathbf{e}_m$, i.e., the masked token, and the uniform diffusion process for $\mathbf{u} = \sum_{i=1}^d \mathbf{e}_i / \sqrt{d}$. \square

Although discrete diffusion processes can be represented as a probability path on the statistical manifold, this flow cannot be learned by a neural network. The network fails to generalize to points outside the geodesic that interpolates the prior and the data distribution, producing an incorrect vector field. While previous works (Cheng et al., 2024; Davis et al., 2024) use the uniform distribution on the simplex as the prior, this does not directly relate to discrete diffusion models. Therefore, we present a simple design for the continuous diffusion model that generalizes existing discrete diffusion models.

3.2. Generative Process on Hypersphere

With the reparameterization, the task of modeling the distribution of discrete data can be reformulated to modeling a distribution on the hypersphere. The reparameterized data distribution p^* can be represented as follows:

$$p^*(x) = \sum_{k=1}^d p_k \delta(x - \mathbf{e}_k), \quad (8)$$

where p_k and \mathbf{e}_k denotes the probability and the one-hot vector of the k -th token, respectively. To model p^* , we build upon the Riemannian Diffusion Mixture framework (Jo & Hwang, 2024) to construct a generative process on the hypersphere. Due to the simple nature of \mathbb{S}^{d-1} , we can derive the logarithm bridge process (Jo & Hwang, 2024) from an arbitrary point $\mathbf{u} \in \mathbb{S}^{d-1}$ to the k -th token \mathbf{e}_k as follows (we provide the derivation in Appendix A.3):

$$\begin{aligned} d\mathbf{X}_t^k &= \gamma_t \frac{\phi_t(\mathbf{e}_k - \cos \phi_t \mathbf{X}_t^k)}{\sin \phi_t} dt + \sigma_t d\mathbf{B}_t^d, \\ \gamma_t &:= \frac{\sigma_t^2}{\int_t^T \sigma_s^2 ds}, \quad \phi_t := \cos^{-1} \langle \mathbf{X}_t^k, \mathbf{e}_k \rangle, \quad \mathbf{X}_0^k = \mathbf{u}, \end{aligned} \quad (9)$$

where \mathbf{B}_t^d denotes the Brownian motion defined on \mathbb{S}^{d-1} and ϕ_t denotes the geodesic distance between the current state and the endpoint.

Intuitively, the current state \mathbf{X}_t moves in the direction that minimizes the geodesic distance to the endpoint, resulting in a process that bridges the starting and end points. While different forms of the bridge process exist, for example, scaling the drift or the diffusion coefficients, Eq. (9) yields a specific transition distribution that enables simulation-free training, which we explain in Section 4.

From the bridge processes, we construct a diffusion process on \mathbb{S}^{d-1} using the diffusion mixture representation (Proposition A.7) with mixing distribution p^* (see Appendix A.4 for the formal definition of the representation):

$$d\mathbf{X}_t = \left[\sum_{k=1}^d p_{T|t}(\mathbf{e}_k | \mathbf{X}_t) \eta^k(\mathbf{X}_t, t) \right] dt + \sigma_t d\mathbf{B}_t^d, \quad (10)$$

where η^k denote the drift of the bridge process in Eq. (9). $p_{T|t}(\mathbf{e}_k | \mathbf{X}_t)$ represents the probability that the token \mathbf{e}_k will be the final outcome of the process, given the current state \mathbf{X}_t at time t . Note that the construction guarantees the terminal distribution of the process to be p^* .

An ideal generative process is one that gradually refines the uninformative states to recover the original tokens. We analyze the convergence of the bridge process through its radial process $r_t^k := d_g(\mathbf{X}_t, \mathbf{e}_k)$ described by the following SDE (see Appendix A.3 for the derivation using Itô’s formula):

$$dr_t^k = \left[-\gamma_t r_t^k + \frac{\sigma_t^2 d}{2} \cot r_t^k \right] dt + \sigma_t dW_t, \quad (11)$$

where W_t is a 1-dimensional Wiener process. For $\sigma_0 > \sigma_T$, the radial process converges rapidly in early time steps, making it difficult for a neural network to approximate accurately. We empirically find that the geometric schedule $\sigma_t = \sigma_0^{1-t} \sigma_T^t$ with $\sigma_0 < \sigma_T$ leads to gradual convergence.

Masked Diffusion From Proposition 3.1, fixing the initial distribution to be the mask token \mathbf{e}_m yields a mixture process that generalizes the masked discrete diffusion process. The resulting process starts from a mask token and moves to one of the tokens following the drift. In the perspective of discrete diffusion, our process smoothly interpolates the jump from the mask token to the final token via through the continuous states \mathbf{X}_t , with $p_{T|t}(\mathbf{e}_k | \mathbf{X}_t)$ determining the direction of the process.

The generalized framework shares similar properties with the masked discrete diffusion (Sahoo et al., 2024): (1) **Zero Mask Probabilities.** Our parameterization in Eq.(16) sets the probability $p_{T|t}(\mathbf{e}_m | \mathbf{X}_t)$ to zero, indicating that the final token cannot be a mask token. (2) **Carry-Over Unmasking.** If \mathbf{X}_t converges to a token \mathbf{e}_k before the terminal time, the

drift in Eq. (9) also converges to zero and the state \mathbf{X}_t is carried over without changing to different token.

Yet, the fundamental difference is that discrete diffusion directly jumps from a token to the mask token and vice versa where a wrong jump is non-revokable, making the generation process uneditable. On the other hand, our continuous approach offers numerous chances to correct wrong directions during the process, leading to a more accurate modeling of the data distribution.

Uniform Diffusion From Proposition 3.1, the generalization of the uniform diffusion can be achieved by setting the starting point to be the barycenter of the simplex mapped to \mathbb{S}^{d-1} , i.e., $\pi\left(\sum_{i=1}^d \mathbf{e}_i/d\right) = \sum_{i=1}^d \mathbf{e}_i/\sqrt{d}$. We further extend the uniform diffusion so that the transition to a subset of tokens \mathcal{S} gets a different probability ζ :

$$\pi\left(\sum_{i \in \mathcal{S}} \zeta \mathbf{e}_i + \sum_{j \notin \mathcal{S}} \frac{1 - \zeta|\mathcal{S}|}{d - |\mathcal{S}|} \mathbf{e}_j\right), \quad 0 \leq \zeta \leq \frac{1}{|\mathcal{S}|}. \quad (12)$$

For $\mathcal{S} = \{m\}$ and $\zeta = 1$, we obtain the masked diffusion.

Mixture Paths Since masked diffusion and uniform diffusion have different initial conditions, they yield different convergence behaviors. We empirically observe that under the same noise schedule, uniform diffusion is easier to learn in the early time steps compared to masked diffusion, whereas the opposite holds in later stages. This suggests that a diffusion process mixing masked and uniform processes could result in an improved generative model.

Therefore, we derive a new family of generative processes by mixing the probability path of generative processes $\{\mathbb{Q}^{*,i} : 1 \leq i \leq n\}$ sharing the same noise schedule σ_t (see Appendix A.4 for detailed derivation of mixture path):

$$\mathbb{Q}_t^{mix} := \sum_{i=1}^n \lambda_t^i \mathbb{Q}_t^{*,i}; \quad \sum_{i=1}^n \lambda_t^i = 1, \quad (13)$$

where λ_t^n denotes the mixing schedule. From the perspective of diffusion mixture representation, this corresponds to creating a mixture of generative processes $\{\mathbb{Q}_t^{*,i}\}$ with mixing distribution λ_t^i .

One example is to create a mixture path from the masked bridges and uniform bridges:

$$\lambda_t \mathbb{Q}_t^{mask} + (1 - \lambda_t) \mathbb{Q}_t^{unif}, \quad (14)$$

with initial distribution $\lambda_0 \delta(\mathbf{e}_m) + (1 - \lambda_0) \delta(\sum_{i=1}^d \mathbf{e}_i/\sqrt{d})$, which generalizes the mixture paths used in discrete flow matching (Shaul et al., 2024).

Generalizing Flow Matching Our framework generalizes flow matching methods on the statistical manifold (Cheng et al., 2024; Davis et al., 2024). By designing the noise schedule in Eq. (9) to be $\sigma_t := \sigma_0 \rightarrow 0$, we obtain the conditional vector field of the flow matching models.

4. Simulation-Free Training with Radial Symmetry

Next, we introduce our training scheme. We derive the likelihood bound for our model and present a simple parameterization and objectives. Further, we present a simulation-free training method based on the radial symmetry of \mathbb{S}^d .

Likelihood Bound Our approach yields a simple form of evidence-lower bound (ELBO) by using the Girsanov theorem on compact manifolds (De Bortoli et al. (2022), Corollary H.3). For a point $\mathbf{z} \in \mathbb{S}^d$, we can upper bound the negative log-likelihood of our model (Eq. (10)) by the KL divergence between the approximated mixture process and the bridge process with endpoint \mathbf{z} :

$$\begin{aligned} -\log p_\theta(\mathbf{z}) &= D_{KL}(\delta(\mathbf{z}) \| p_\theta(\mathbf{X}_T) = \mathbf{z}) \leq D_{KL}(\mathbb{Q}^z \| \mathbb{Q}^\theta) \\ &= \mathbb{E}_{\mathbf{X} \sim \mathbb{Q}^z} \left[\frac{1}{2} \int_0^T \left\| \sigma_t^{-1} (\eta^\theta(\mathbf{X}_t, t) - \eta^z(\mathbf{X}_t, t)) \right\|^2 dt \right] \end{aligned}$$

where \mathbb{Q}^z and \mathbb{Q}^θ denote the probability measure of the bridge and mixture processes, respectively, and η^θ denotes the drift of Eq. (10). The point-wise likelihood bound provides an upper bound on the NLL $\mathbb{E}_{\mathbf{z} \sim p^*} [-\log p_\theta(\mathbf{z})]$:

$$\mathbb{E}_{\substack{\mathbf{e}_k \sim p^* \\ \mathbf{X} \sim \mathbb{Q}^k}} \left[\frac{1}{2} \int_0^T \left\| \sigma_t^{-1} (\eta^\theta(\mathbf{X}_t, t) - \eta^k(\mathbf{X}_t, t)) \right\|^2 dt \right], \quad (15)$$

where \mathbb{Q}^k and η^k denote the probability measure and the drift of the bridge process with endpoint \mathbf{e}_k , respectively.

Parameterization and Objective The drift of the mixture process diverges near the terminal time, which makes it challenging to learn. Therefore, instead of approximating the drift function directly, we propose to model the probability $p_{T|t}(\mathbf{X}_T | \mathbf{X}_t)$ with a neural network \mathbf{s}_θ as follows:

$$\begin{aligned} p_\theta(\mathbf{X}_t, t) &:= \text{softmax}(\mathbf{s}_\theta(\mathbf{X}_t, t)) \\ &= \left[p_{T|t}(\mathbf{e}_1 | \mathbf{X}_t), \dots, p_{T|t}(\mathbf{e}_d | \mathbf{X}_t), 0 \right]^\top, \end{aligned} \quad (16)$$

where we force the probability $p_{T|t}(\mathbf{e}_m | \mathbf{X}_t)$ to be zero. Then the drift of the mixture process can be represented by the parameterization as follows:

$$\eta^\theta(\mathbf{X}_t, t) = \sum_{k=1}^d \left\langle p_\theta(\mathbf{X}_t, t), \mathbf{e}_k \right\rangle \eta^k(\mathbf{X}_t, t), \quad (17)$$

Based on the ELBO of Eq. (15), we derive a maximum likelihood training objective with the parameterized drift:

$$\mathcal{L}(\theta) = \mathbb{E}_{\substack{e_k \sim p^* \\ \mathbf{X} \sim \mathbb{Q}^k}} \left[\frac{1}{2} \int_0^T \sigma_t^{-2} E_\theta^k(\mathbf{X}_t, t) dt \right] \quad (18)$$

$$E_\theta^k(x, t) = \left\| \sum_{l=1}^d \langle p_\theta(x, t), e_l \rangle \eta^l(x, t) - \eta^k(x, t) \right\|^2,$$

which can be interpreted as minimizing the mean squared error of the drift approximation.

A key observation is that ELBO can be minimized by reducing the cross-entropy between the probability vector $p_\theta(\mathbf{X}_t, t)$ and the target one-hot vector e_k . Therefore we introduce a cross-entropy-based training objective similar to that used in discrete diffusion models (Sahoo et al., 2024; Shi et al., 2024):

$$\mathcal{L}^{CE}(\theta) = \mathbb{E}_{\substack{e_k \sim p^* \\ \mathbf{X} \sim \mathbb{Q}^k}} \left[\int_0^T -\log \langle p_\theta(\mathbf{X}_t, t), e_k \rangle dt \right]. \quad (19)$$

We experimentally find that the cross-entropy-based loss yields faster convergence in training and leads to better performance than the mean squared error-based loss.

Importance Sampling The difficulty of approximating the probability $p_{T|t}(\mathbf{X}_T|\mathbf{X}_t)$ varies significantly across different time points t . While predicting \mathbf{X}_T is fairly easy in the later stage of the process, it is challenging to do so during the middle of the process. The training objective can be improved by training more on the challenging time points. We achieve this by using an importance sampling technique on t which modifies the time distribution to focus on a specific interval, resulting in an equivalent objective:

$$\mathcal{L}_q(\theta) = \mathbb{E}_{\substack{e_k \sim p^* \\ \mathbf{X} \sim \mathbb{Q}^k}} \mathbb{E}_{t \sim q} \left[-q(t) \log \langle p_\theta(\mathbf{X}_t, t), e_k \rangle \right] \quad (20)$$

where q is the normalized proposal distribution for t . We find that a simple density $q(t) = 1 - \epsilon$ if $t \in [a, b]$ else ϵ to be effective.

Approximation of Transition Distribution The training objective requires sampling \mathbf{X}_t from the bridge processes at each iteration. Since the diffusion process on the d -dimensional sphere does not yield a tractable transition distribution, it requires simulating the process which becomes a significant bottleneck during training. Therefore, we introduce an approximation sampling method that enables simulation-free training, which makes our framework scalable to a large vocabulary.

We approximate the distribution $p(\mathbf{X}_t|\mathbf{X}_0, \mathbf{X}_T)$ as the push-forward measure of a Gaussian distribution on the tangent space by the exponential map, i.e., the Riemannian normal.

This is possible since Eq. (9) is obtained by applying the time change (Øksendal, 2003) to a simple bridge:

$$d\hat{\mathbf{X}}_t = \frac{1}{T-t} \frac{\phi_t(e_k - \cos \phi_t \hat{\mathbf{X}}_t)}{\sin \phi_t} dt + d\mathbf{B}_t^d, \quad (21)$$

for $\phi_t := \cos^{-1} \langle \hat{\mathbf{X}}_T, \hat{\mathbf{X}}_t \rangle$, which yields a transition distribution similar to Riemannian normal.

We parameterize the mean μ_t and the covariance Σ_t of the Riemannian normal approximating $p(\mathbf{X}_t|\mathbf{X}_0=\mathbf{u}, \mathbf{X}_T=\mathbf{v})$ with the parameters α_t and ρ_t as follows:

$$\mu_t = \frac{\mathbb{E} \mathbf{X}_t}{\|\mathbb{E} \mathbf{X}_t\|} = \frac{\alpha_t}{\sin \phi_0} \mathbf{v} + \left(\sqrt{1 - \alpha_t^2} - \frac{\alpha_t \cos \phi_0}{\sin \phi_0} \right) \mathbf{u}$$

$$\Sigma_t = \text{Cov} [\exp_{\mu_t}^{-1}(\mathbf{X}_t)] = \rho_t^2 \mathbf{I}, \quad (22)$$

for $\phi_0 := \cos^{-1} \langle \mathbf{u}, \mathbf{v} \rangle$. Intuitively, μ_t represents the normalized centroid of the samples \mathbf{X}_t and $\rho_t^2 \mathbf{I}$ corresponds to the covariance of the lifted samples in the tangent space \mathcal{T}_{μ_t} .

Connection to Projected Processes While the parameters α_t and ρ_t are generally intractable, we derive them from the 1-dimensional projections of the diffusion process. Our main idea is to represent the parameters using the projected processes $c_t^w := \langle \mathbf{X}_t, \mathbf{w} \rangle$ for $\mathbf{w} = \mathbf{X}_0$ and \mathbf{X}_1 .

For a bridge process from \mathbf{u} to \mathbf{v} , the projected process $c_t^v = \langle \mathbf{X}_t, \mathbf{v} \rangle$ is modeled by a 1-dimensional SDE derived from the Itô's formula and the radial symmetry of \mathbb{S}^d (see Appendix A.5 for the derivation):

$$dc_t^v = b(c_t^v, t)dt + \sigma_t \sqrt{1 - (c_t^v)^2} dW_t,$$

$$b(c, t) = \gamma_t \cos^{-1} c \sqrt{1 - c^2} - \frac{d\sigma_t^2}{2} c \quad (23)$$

where W_t is a 1-dimensional standard Wiener process. Similarly, $c_t^u = \langle \mathbf{X}_t, \mathbf{u} \rangle$ is described by a SDE that depends on c_t^v (see Appendix A.5 for the derivation):

$$dc_t^u = \tilde{b}(c_t^u, c_t^v, t)dt + \sigma_t \sqrt{1 - (c_t^u)^2} dW_t, \quad (24)$$

$$\tilde{b}(c^u, c^v, t) = \gamma_t \frac{\cos^{-1} c^v}{\sqrt{1 - (c^v)^2}} \left(\langle \mathbf{u}, \mathbf{v} \rangle - c^u c^v \right) - \frac{d\sigma_t^2}{2} c^u$$

From the initial conditions $c_0^v = \langle \mathbf{u}, \mathbf{v} \rangle$ and $c_0^u = 1$, we obtain the connection between the projections and the parameters of Riemannian normal (see Appendix A.6):

$$\mathbb{E} c_t^v = \left(\sqrt{1 - \langle \mathbf{u}, \mathbf{v} \rangle^2} \alpha_t + \langle \mathbf{u}, \mathbf{v} \rangle \sqrt{1 - \alpha_t^2} \right) F_d(\rho_t),$$

$$\mathbb{E} c_t^u = \sqrt{1 - \alpha_t^2} F_d(\rho_t), \quad F_d(\rho) := e^{-\frac{\rho^2}{2}} {}_1F_1 \left(\frac{d}{2}, \frac{1}{2}, -\frac{\rho^2}{2} \right)$$

where ${}_1F_1$ denotes the confluent hypergeometric function. Therefore, the parameters of the Riemannian normal can be

derived from the mean projections $\mathbb{E}c_t^u$ and $\mathbb{E}c_t^v$ as follows:

$$\alpha_t = \sqrt{\frac{(r_t - \langle u, v \rangle)^2}{1 - \langle u, v \rangle^2 + (r_t - \langle u, v \rangle)^2}}, \quad r_t = \frac{\mathbb{E}c_t^v}{\mathbb{E}c_t^u} \quad (25)$$

$$\rho_t = F_d^{-1} \left(\mathbb{E}c_t^u / \sqrt{1 - \alpha_t^2} \right),$$

where F_d^{-1} denotes the inverse function of F_d . For small d , we calibrate ρ_t by scaling up with a constant.

While the mean projections $\mathbb{E}c_t^u$ and $\mathbb{E}c_t^v$ generally do not have closed-form solutions, they can be easily obtained from simulating the 1-dimensional processes Eq. (23) and Eq. (24). In particular, for masked and uniform diffusion, u is fixed to a single point for which $\langle u, e_k \rangle$ is the same for all the non-masked tokens. Due to the radial symmetry, $\mathbb{E}c_t^{e_k}$ is identical for all k and the bridge processes \mathbb{Q}^k share the same α_t and ρ_t .

Therefore, before training our model, we pre-compute α_{t_i} and ρ_{t_i} only once for $t_i := i/N$ with sufficiently large N , by simulating the 2-dimensional process $(c_t^u, c_t^{e_1})$. Then with the pre-computed parameters, we can easily sample X_t from the Riemannian normal during training without expensive simulation of the bridge processes, achieving $\times 50$ faster speed up compared to the simulation-based training. We experimentally demonstrate that our approach provides an accurate approximation of the distribution X_t in Section 7.4.

5. Generation of Token Sequences

Sequence of Tokens Now we generalize the result of single token modeling to the generation of token sequences. Since each token in the sequence is reparameterized to d -dimensional spheres, a sequence of length n is modeled on a product manifold $(\mathbb{S}^d)^n := \mathbb{S}^d \times \dots \times \mathbb{S}^d$. The diffusion processes on each hypersphere are dependent on each other, described by the following system of SDEs:

$$dX_t^i = \sum_{k=1}^d p(X_T^i = e_k | X_t^{1:n}) \eta^k(X_t^i, t) + \sigma_t dB_t^d, \quad (26)$$

for $1 \leq i \leq n$, where η^k denotes the drift of the bridge on \mathbb{S}^d with endpoint e_k . Note that $p(X_T^i = e_k | X_t^{1:n})$ denotes the probability of the i -th token being the k -th state which relies on the current intermediate sequence $X_t^{1:n}$, and we train a neural network to predict the probabilities.

Our framework allows generating sequences of arbitrary lengths smaller than the maximum length. Using the tokens [BOS] and [EOS] that denote the start and the end of the sequence, we can generate a sequence of the desired length by fixing the position of these tokens.

Dimension Splitting of Statistical Manifold For a large vocabulary set, the corresponding statistical manifold has a

high dimension which results in two challenges: (1) **Abrupt convergence**. Bridge processes on a high-dimensional sphere converge abruptly near the end of the process, which makes them hard to learn with a neural network. (2) **Large input dimension**. Since the input of the network is of high dimension, the hidden dimensions of the network should be sufficiently large to encode them properly. Models with small capacity fail to learn the probabilities of Eq.(16).

To address these challenges, we introduce *dimension splitting*, a simple technique to reduce the dimension of the parameterized manifold. Instead of directly mapping the k -th token to \mathbb{S}^d , we represent the index k in base b which is then mapped to the product manifold $(\mathbb{S}^{\tilde{b}})^m$ where $\tilde{b} = b$ for masked diffusion and otherwise $b - 1$, and $m := \lceil \log_b d \rceil$. Dimension splitting reparameterizes a sequence of length L to a product manifold $(\mathbb{S}^{\tilde{b}})^{mL}$, and the bridge processes defined on $\mathbb{S}^{\tilde{b}}$ with small \tilde{b} yield gradual convergence that can be easily learned by a neural network. Dimension splitting significantly enhances the likelihood of our model when used together with the mixture path (Eq. (14)).

6. Related Work

Discrete Diffusion Models Discrete diffusion directly models the Markov chain on discrete data space. The one-hot data distribution is gradually corrupted to a stationary distribution with specific transition matrices, where the noising process corresponds to the stochastic jumps between states in the Markov chain. D3PM (Austin et al., 2021) introduces discrete-time Markov forward processes with uniform and absorbing state transition matrices and has been generalized to continuous-time Markov chain framework (Campbell et al., 2022). SEDD (Lou et al., 2024) proposes learning the score entropy of the discrete states instead of the mean prediction. Recent works (Shi et al., 2024; Sahoo et al., 2024) introduce continuous-time masked diffusion models with a simpler form of likelihood bounds.

Continuous Diffusion Models for Discrete Data Early works approached by fully relaxing the discrete data into continuous space (Han et al., 2022) or embedding the tokens in a latent space (Li et al., 2022; Dieleman et al., 2022), without any constraint. However, continuous relaxation without constraint fails to accurately model the discreteness of the categorical distribution. Recent works utilize the logit space (Hoogeboom et al., 2021; Graves et al., 2023) or the probability simplex (Avdeyev et al., 2023; Stärk et al., 2024) based on the Dirichlet distribution, which require strong assumptions on the diffusion noising processes. Flow matching has been applied to the probability simplex by using the statistical manifold on categorical distribution (Cheng et al., 2024; Davis et al., 2024) but has limited performance lagging behind discrete diffusion models.

Table 1: **Bits Per Character (BPC)** results on Text8 test set. Results are taken from the corresponding papers. Bold denotes the best result in autoregressive or diffusion models.

| Method | BPC (\downarrow) |
|---------------------------------|----------------------|
| <i>Autoregressive</i> | |
| IAF/SCF | 1.88 |
| AR Argmax Flow | 1.39 |
| Transformer AR | 1.23 |
| Discrete Flow | 1.23 |
| <i>Any-order Autoregressive</i> | |
| ARDM | ≤ 1.43 |
| MAC | ≤ 1.40 |
| <i>Discrete Diffusion</i> | |
| Multinomial Diffusion | ≤ 1.72 |
| D3PM Uniform | ≤ 1.61 |
| D3PM Absorb | ≤ 1.45 |
| SEDD Absorb | ≤ 1.39 |
| MDLM | ≤ 1.40 |
| MD4 | ≤ 1.37 |
| <i>Continuous Diffusion</i> | |
| Plaid | ≤ 1.48 |
| BFN | ≤ 1.41 |
| RDLM (Ours) | \leq 1.32 |

7. Experiments

7.1. Text Generation

We evaluate our Riemannian Diffusion Language Model (RDLM) for text generation tasks on two language benchmarks: Text8 (Mahoney, 2006) and One Billion Words Dataset (Chelba et al., 2013).

Baselines We compare against state-of-the-art autoregressive and diffusion models. Multinomial Diffusion (Hoogeboom et al., 2021), D3PM (Austin et al., 2021), SEDD (Lou et al., 2024), MDLM (Sahoo et al., 2024), MD4 (Shi et al., 2024) are discrete diffusion models. Plaid (Gulrajani & Hashimoto, 2024) and Bayesian Flow Network (BFN) (Graves et al., 2023) are continuous diffusion models. IAF/SCF (Ziegler & Rush, 2019), AR Argmax Flow (Hoogeboom et al., 2021), and Discrete Flow (Tran et al., 2019) are flow-based models, and ARDM (Hoogeboom et al., 2022) and MAC (Shih et al., 2022) are any-order autoregressive models. We also compare with transformer AR model (Vaswani et al., 2017). We provide further details on the baselines in Appendix B.1

Implementation Details For all experiments, we use the same data split and context size following Lou et al. (2024) and Sahoo et al. (2024). For Text8, we randomly sample contiguous chunks of length 256 as done in previous works (Austin et al., 2021; Lou et al., 2024). For One Bil-

Table 2: **Test perplexity (PPL)** results on LM1B dataset. Baseline results are taken from Sahoo et al. (2024).

| Method | # Param. | PPL (\downarrow) |
|-----------------------------|----------|----------------------|
| <i>Autoregressive</i> | | |
| Transformer-X Base | 0.46B | 23.5 |
| OmniNet _r | 100M | 21.5 |
| Transformer | 110M | 22.32 |
| <i>Discrete Diffusion</i> | | |
| BERT-Mouth | 110M | ≤ 142.89 |
| D3PM Absorb | 70M | ≤ 76.90 |
| DiffusionBert | 110M | ≤ 63.78 |
| SEDD | 110M | ≤ 32.79 |
| MDLM | 110M | ≤ 27.04 |
| <i>Continuous Diffusion</i> | | |
| Diffusion-LM | 80M | ≤ 118.62 |
| RDLM (Ours) | 110M | ≤ 29.72 |

lion Words, we use the same tokenizer as in He et al. (2023) with context size 128. We use a diffusion transformer architecture (Peebles & Xie, 2023) with rotary positional embeddings (Su et al., 2024) for all the experiments and match the number of parameters as used in the previous works (Lou et al., 2024; Sahoo et al., 2024). For our model, we use the mixture path of masked and uniform diffusion (Eq. (14)) and apply dimension splitting for large vocabulary. We provide more details in Appendix B.1.

Text8 We first evaluate on a small character-level language modeling task. Text8 (Mahoney, 2006) dataset is a character-level text modeling benchmark extracted from English Wikipedia. We train the models on short text chunks of length 256 and evaluate the models using Bits Per Character (BPC). As shown in Table 1, our framework outperforms all previous diffusion models, both the discrete and continuous methods. We also outperform the any-order autoregressive models that generate texts in flexible decoding order similar to discrete diffusion models. We achieve similar generative perplexity and entropy compared to existing discrete diffusion models. We provide the generated texts from RDLM in Appendix C.1.

One Billion Words We further evaluate on One Billion Words Dataset (LM1B) (Chelba et al., 2013), a medium-sized real-world language benchmark. We evaluate the models using perplexity (PPL) and the results are summarized in Table 2. RDLM outperforms most of the diffusion models and is comparable to the state-of-the-art discrete diffusion model (Shi et al., 2024). In particular, we significantly outperform the existing continuous diffusion model (Li et al., 2022) demonstrating the effectiveness of incorporating the geometry of the underlying categorical distribution. We provide the generated texts in Appendix C.2.

Table 3: **Bits Per Dimension (BPD)** results on CIFAR-10 dataset. Baseline results are taken from Shi et al. (2024).

| Method | # Param. | BPD (\downarrow) |
|-----------------------------|----------|----------------------|
| <i>Autoregressive</i> | | |
| PixelRNN | | 3.00 |
| Gated PixelCNN | | 3.03 |
| PixelCNN++ | 53M | 2.92 |
| PixelSNAIL | 46M | 2.85 |
| Image Transformer | | 2.90 |
| Sparse Transformer | 59M | 2.80 |
| <i>Discrete Diffusion</i> | | |
| D3PM Absorb | 37M | ≤ 4.40 |
| D3PM Gauss | 36M | ≤ 3.44 |
| τ LDR | 36M | ≤ 3.59 |
| MD4 | 28M | ≤ 2.78 |
| <i>Continuous Diffusion</i> | | |
| RDLM (Ours) | 35M | ≤ 2.74 |

7.2. Pixel-level Image Modeling

We further explore applications beyond the text domain. We train our model on order-agnostic image data where each image is represented as a set of discrete tokens with a vocabulary of size 256. This removes the information of relative proximity between different pixels. We compare RDLM against autoregressive models and discrete diffusion models that directly work on raw pixel space, which we describe in Appendix B.2. As shown in Table 3, our method achieves the lowest BPD outperforming the discrete diffusion models (Austin et al., 2021; Shi et al., 2024) and autoregressive models (Chen et al., 2018; Child et al., 2019).

7.3. DNA Sequence Design

We show that our framework can be applied to the generation of biological sequences. We evaluate our method for the promoter DNA sequence design task, which aims to generate valid promoter DNA sequences conditioned on transcription profiles. We provide further details of the task in Appendix B.3. We measure the mean squared error (MSE) between the predicted regulatory activity of the generated sequence and that of the original sequence corresponding to the transcription profile. Table 4 shows that our framework achieves the lowest MSE, outperforming the flow matching methods (Stärk et al., 2024; Davis et al., 2024) and the discrete diffusion diffusion model (Austin et al., 2021).

7.4. Analysis

Approximation of Transition Distribution In Figure 3, we measure the maximum mean discrepancy (MMD) (Gretton et al., 2012) distance between the simulated transition distribution and the approximated distribution. The approximated distributions show almost the same MMD as the

Table 4: **MSE** results on the generated promoter DNA sequences. Baseline results are taken from Davis et al. (2024).

| Method | MSE (\downarrow) |
|-------------------------|----------------------|
| Bit-Diffusion (bit) | 0.041 |
| Bit-Diffusion (one-hot) | 0.040 |
| D3PM Uniform | 0.038 |
| DDSM | 0.033 |
| DirichletFM | 0.034 |
| Language Model | 0.034 |
| Fisher-Flow | 0.029 |
| RDLM (Ours) | 0.027 |

simulated distributions, indicating that the approximation is reliable. In particular, the discrepancy becomes close to zero in the high-dimensional manifold, where the simulation of the SDE becomes expensive.

Training Objective We validate the effectiveness of the cross-entropy-based loss of Eq. (19) in Table 1. Compared to the mean-squared error-based loss of Eq. (18), the cross-entropy loss provides faster convergence in training and better NLL. Furthermore, Table 1 shows that applying importance sampling (Eq. (20)) improves the performance.

Dimension Splitting For datasets with a large vocabulary, for example, LM1B dataset, splitting the dimension of the manifold yields a significant improvement. Table 2 shows that the generative model on the high-dimensional manifold cannot be trained due to the large input dimension. While adding additional information to the model does improve the result, the abrupt convergence of bridge processes on high dimensions makes them challenging to learn. For a large vocabulary, we achieve the best result by splitting the dimensions into smaller ones and modeling the generative process using a mixture path.

8. Conclusion

In this work, we introduced Riemannian Diffusion Language Model (RDLM), a continuous diffusion model for language and discrete data. We present a simple framework that generalizes discrete diffusion models building on the connection between the transition distribution of the diffusion process and the probability path on the statistical manifold. We provide general designs of the diffusion processes and introduce a simulation-free training scheme leveraging the radial symmetry of the hypersphere. We validate through experiments on language benchmarks that RDLM outperforms previous discrete and continuous diffusion models for language modeling. Further, we explore applications to other modalities including images and biological sequences achieving state-of-the-art results.

Impact Statement This paper presents work whose goal is to advance the field of deep generative models for language modeling and discrete data. We believe our work can enhance our understanding of various scientific fields dealing with discrete data.

References

- Amari, S.-i. *Information geometry and its applications*, volume 194. Springer, 2016.
- Austin, J., Johnson, D. D., Ho, J., Tarlow, D., and Van Den Berg, R. Structured denoising diffusion models in discrete state-spaces. In *Advances in Neural Information Processing Systems*, 2021.
- Avdeyev, P., Shi, C., Tan, Y., Dudnyk, K., and Zhou, J. Dirichlet diffusion score model for biological sequence generation. In *International Conference on Machine Learning*, 2023.
- Ay, N., Jost, J., Vn Lê, H., and Schwachhöfer, L. *Information geometry*, volume 64. Springer, 2017.
- Brooks, T., Peebles, B., Holmes, C., DePue, W., Guo, Y., Jing, L., Schnurr, D., Taylor, J., Luhman, T., Luhman, E., et al. Video generation models as world simulators, 2024.
- Campbell, A., Benton, J., De Bortoli, V., Rainforth, T., Deligiannidis, G., and Doucet, A. A continuous time framework for discrete denoising models. In *Advances in Neural Information Processing Systems*, 2022.
- Chelba, C., Mikolov, T., Schuster, M., Ge, Q., Brants, T., Koehn, P., and Robinson, T. One billion word benchmark for measuring progress in statistical language modeling. *arXiv preprint arXiv:1312.3005*, 2013.
- Chen, T., Zhang, R., and Hinton, G. E. Analog bits: Generating discrete data using diffusion models with self-conditioning. In *International Conference on Learning Representation*, 2023.
- Chen, X., Mishra, N., Rohaninejad, M., and Abbeel, P. Pixelsnail: An improved autoregressive generative model. In *International Conference on Machine Learning*, 2018.
- Cheng, C., Li, J., Peng, J., and Liu, G. Categorical flow matching on statistical manifolds. In *Advances in Neural Information Processing Systems*, 2024.
- Child, R., Gray, S., Radford, A., and Sutskever, I. Generating long sequences with sparse transformers. *arXiv:1904.10509*, 2019.
- Davis, O., Kessler, S., Petrache, M., Ceylan, İ. İ., Bronstein, M. M., and Bose, A. J. Fisher flow matching for generative modeling over discrete data. In *Advances in Neural Information Processing Systems*, 2024.
- De Bortoli, V., Mathieu, E., Hutchinson, M., Thornton, J., Teh, Y. W., and Doucet, A. Riemannian score-based generative modelling. In *Advances in Neural Information Processing Systems*, 2022.
- Dhariwal, P. and Nichol, A. Q. Diffusion models beat gans on image synthesis. In *Advances in Neural Information Processing Systems*, 2021.
- Dieleman, S., Sartran, L., Roshannai, A., Savinov, N., Ganin, Y., Richemond, P. H., Doucet, A., Strudel, R., Dyer, C., Durkan, C., et al. Continuous diffusion for categorical data. *arXiv:2211.15089*, 2022.
- Esser, P., Kulal, S., Blattmann, A., Entezari, R., Müller, J., Saini, H., Levi, Y., Lorenz, D., Sauer, A., Boesel, F., Podell, D., Dockhorn, T., English, Z., and Rombach, R. Scaling rectified flow transformers for high-resolution image synthesis. In *International Conference on Machine Learning*, 2024.
- Gat, I., Remez, T., Shaul, N., Kreuk, F., Chen, R. T. Q., Synnaeve, G., Adi, Y., and Lipman, Y. Discrete flow matching. In *Advances in Neural Information Processing Systems*, 2024.
- Graves, A., Srivastava, R. K., Atkinson, T., and Gomez, F. Bayesian flow networks. *arXiv:2308.07037*, 2023.
- Gretton, A., Borgwardt, K. M., Rasch, M. J., Schölkopf, B., and Smola, A. A kernel two-sample test. *The Journal of Machine Learning Research*, 13(1):723–773, 2012.
- Gulrajani, I. and Hashimoto, T. B. Likelihood-based diffusion language models. In *Advances in Neural Information Processing Systems*, 2024.
- Han, X., Kumar, S., and Tsvetkov, Y. Ssd-lm: Semi-autoregressive simplex-based diffusion language model for text generation and modular control. *arXiv:2210.17432*, 2022.
- He, Z., Sun, T., Tang, Q., Wang, K., Huang, X., and Qiu, X. Diffusionbert: Improving generative masked language models with diffusion models. In *Annual Meeting of the Association for Computational Linguistics*, 2023.
- Ho, J. and Salimans, T. Classifier-free diffusion guidance. *arXiv:2207.12598*, 2022.
- Hon, C.-C., Ramilowski, J. A., Harshbarger, J., Bertin, N., Rackham, O. J., Gough, J., Denisenko, E., Schmeier, S., Poulsen, T. M., Severin, J., et al. An atlas of human long non-coding rnas with accurate 5 ends. *Nature*, 543(7644): 199–204, 2017.
- Hoogetboom, E., Nielsen, D., Jaini, P., Forré, P., and Welling, M. Argmax flows and multinomial diffusion: Learning

- categorical distributions. In *Advances in Neural Information Processing Systems*, 2021.
- Hoogeboom, E., Gritsenko, A. A., Bastings, J., Poole, B., Berg, R. v. d., and Salimans, T. Autoregressive diffusion models. In *International Conference on Learning Representation*, 2022.
- Hsu, E. P. *Stochastic analysis on manifolds*. Number 38 in Graduate studies in mathematics. American Mathematical Society, 2002.
- Jo, J. and Hwang, S. J. Generative modeling on manifolds through mixture of riemannian diffusion processes. In *International Conference on Machine Learning*, 2024.
- Jo, J., Kim, D., and Hwang, S. J. Graph generation with diffusion mixture. In *International Conference on Machine Learning*, 2024.
- Jung, H., Park, Y., Schmid, L., Jo, J., Lee, D., Kim, B., Yun, S., and Shin, J. Conditional synthesis of 3d molecules with time correction sampler. In *Advances in Neural Information Processing Systems*, 2024.
- Li, X., Thickstun, J., Gulrajani, I., Liang, P. S., and Hashimoto, T. B. Diffusion-lm improves controllable text generation. In *Advances in Neural Information Processing Systems*, 2022.
- Loshchilov, I. and Hutter, F. Decoupled weight decay regularization. *arXiv:1711.05101*, 2017.
- Lou, A., Meng, C., and Ermon, S. Discrete diffusion language modeling by estimating the ratios of the data distribution. In *International Conference on Machine Learning*, 2024.
- Mahoney, M. Large text compression benchmark. <https://www.matmahoney.net/dc/text.html>, 2006. .
- Parmar, N., Vaswani, A., Uszkoreit, J., Kaiser, L., Shazeer, N., Ku, A., and Tran, D. Image transformer. In *International Conference on Machine Learning*, 2018.
- Peebles, W. and Xie, S. Scalable diffusion models with transformers. In *Proceedings of the IEEE/CVF International Conference on Computer Vision*, 2023.
- Peluchetti, S. Non-denoising forward-time diffusions. *Openreview*, 2021.
- Polyak, A., Zohar, A., Brown, A., Tjandra, A., Sinha, A., Lee, A., Vyas, A., Shi, B., Ma, C., Chuang, C., Yan, D., Choudhary, D., Wang, D., Sethi, G., Pang, G., Ma, H., Misra, I., Hou, J., Wang, J., Jagadeesh, K., Li, K., Zhang, L., Singh, M., Williamson, M., Le, M., Yu, M., Singh, M. K., Zhang, P., Vajda, P., Duval, Q., Girdhar, R., Sumbaly, R., Rambhatla, S. S., Tsai, S. S., Azadi, S., Datta, S., Chen, S., Bell, S., Ramaswamy, S., Sheynin, S., Bhattacharya, S., Motwani, S., Xu, T., Li, T., Hou, T., Hsu, W., Yin, X., Dai, X., Taigman, Y., Luo, Y., Liu, Y., Wu, Y., Zhao, Y., Kirstain, Y., He, Z., He, Z., Pumarola, A., Thabet, A. K., Sanakoyeu, A., Mallya, A., Guo, B., Araya, B., Kerr, B., Wood, C., Liu, C., Peng, C., Vengertsev, D., Schönfeld, E., Blanchard, E., Juefei-Xu, F., Nord, F., Liang, J., Hoffman, J., Kohler, J., Fire, K., Sivakumar, K., Chen, L., Yu, L., Gao, L., Georgopoulos, M., Moritz, R., Sampson, S. K., Li, S., Parmeggiani, S., Fine, S., Fowler, T., Petrovic, V., and Du, Y. Movie gen: A cast of media foundation models. *arXiv:2410.13720*, 2024.
- Rao, C. R. Information and the accuracy attainable in the estimation of statistical parameters. In *Breakthroughs in Statistics: Foundations and basic theory*, pp. 235–247. Springer, 1992.
- Saharia, C., Chan, W., Saxena, S., Li, L., Whang, J., Denton, E. L., Ghasemipour, S. K. S., Lopes, R. G., Ayan, B. K., Salimans, T., Ho, J., Fleet, D. J., and Norouzi, M. Photorealistic text-to-image diffusion models with deep language understanding. In *Advances in Neural Information Processing Systems*, 2022.
- Sahoo, S. S., Arriola, M., Gokaslan, A., Marroquin, E. M., Rush, A. M., Schiff, Y., Chiu, J. T., and Kuleshov, V. Simple and effective masked diffusion language models. In *Advances in Neural Information Processing Systems*, 2024.
- Salimans, T., Karpathy, A., Chen, X., and Kingma, D. P. Pixelcnn++: Improving the pixelcnn with discretized logistic mixture likelihood and other modifications. In *International Conference on Learning Representations*, 2017.
- Shaul, N., Gat, I., Havasi, M., Severo, D., Sriram, A., Hold-errieth, P., Karrer, B., Lipman, Y., and Chen, R. T. Flow matching with general discrete paths: A kinetic-optimal perspective. *arXiv:2412.03487*, 2024.
- Shi, J., Han, K., Wang, Z., Doucet, A., and Titsias, M. K. Simplified and generalized masked diffusion for discrete data. In *Advances in Neural Information Processing Systems*, 2024.
- Shih, A., Sadigh, D., and Ermon, S. Training and inference on any-order autoregressive models the right way. In *Advances in Neural Information Processing Systems*, 2022.
- Stärk, H., Jing, B., Wang, C., Corso, G., Berger, B., Barzilay, R., and Jaakkola, T. S. Dirichlet flow matching with applications to DNA sequence design. In *International Conference on Machine Learning*, 2024.

- Su, J., Ahmed, M., Lu, Y., Pan, S., Bo, W., and Liu, Y. Roformer: Enhanced transformer with rotary position embedding. *Neurocomputing*, 568:127063, 2024.
- Tran, D., Vafa, K., Agrawal, K. K., Dinh, L., and Poole, B. Discrete flows: Invertible generative models of discrete data. In *Advances in Neural Information Processing Systems*, 2019.
- van den Oord, A., Kalchbrenner, N., Espeholt, L., Kavukcuoglu, K., Vinyals, O., and Graves, A. Conditional image generation with pixelcnn decoders. In *Advances in Neural Information Processing Systems*, 2016a.
- van den Oord, A., Kalchbrenner, N., and Kavukcuoglu, K. Pixel recurrent neural networks. In *International Conference on Machine Learning*, 2016b.
- Vaswani, A., Shazeer, N., Parmar, N., Uszkoreit, J., Jones, L., Gomez, A. N., Kaiser, L., and Polosukhin, I. Attention is all you need. In *Advances in Neural Information Processing Systems*, pp. 5998–6008, 2017.
- Ziegler, Z. M. and Rush, A. M. Latent normalizing flows for discrete sequences. In *International Conference on Machine Learning*, 2019.
- Øksendal, B. *Stochastic Differential Equations*. Universitext. Springer Berlin Heidelberg, 2003.

Appendix

A. Derivations

A.1. Preliminaries

Statistical Manifold of Categorical Distributions For a discrete sample space $\mathcal{X} = \{1, 2, \dots, d\}$, a d -class categorical distribution over \mathcal{X} is parameterized by d number of parameters $p_1, \dots, p_d \geq 0$ such that $\sum_{i=1}^d p_i = 1$. The parameter space corresponds to the $(d-1)$ -dimensional probability simplex:

$$\Delta^{d-1} := \{(p_1, \dots, p_d) \in \mathbb{R}^d \mid \sum_{i=1}^d p_i = 1, p_i \geq 0\}, \quad (27)$$

A natural choice of a Riemannian metric on the simplex is the Fisher-Rao metric (Rao, 1992; Amari, 2016). For an interior point $\mathbf{p} \in \Delta^{d-1}$, the Fisher-Rao metric is defined as follows:

$$g_{FR}(\mathbf{p})[\mathbf{x}, \mathbf{y}] := \langle \mathbf{x}, \mathbf{y} \rangle_{\mathbf{p}} := \left\langle \frac{\mathbf{x}}{\sqrt{\mathbf{p}}}, \frac{\mathbf{y}}{\sqrt{\mathbf{p}}} \right\rangle = \sum_{i=1}^d \frac{x_i y_i}{p_i}, \quad \mathbf{x}, \mathbf{y} \in \mathcal{T}_{\mathbf{p}} \Delta^{d-1}, \quad (28)$$

where the normalization by $\sqrt{\mathbf{p}}$ in the inner product is performed component-wise. This induces a geodesic distance on the simplex defined as follows:

$$d(\mathbf{p}, \mathbf{q}) = 2 \cos^{-1} \left(\sum_{i=1}^d \sqrt{p_i q_i} \right), \quad \mathbf{p}, \mathbf{q} \in \Delta^{d-1}, \quad (29)$$

where \mathbf{p} and \mathbf{q} corresponds to the parameters of categorical distributions. The probability simplex Δ^{d-1} equipped with the Fisher-Rao metric is a Riemannian manifold called the statistical manifold of categorical distribution, denoted as $\mathcal{P}(\mathcal{X})$ throughout the paper. The tangent space at an interior point \mathbf{p} is identified as $\mathcal{T}_{\mathbf{p}}(\mathcal{P}(\mathcal{X})) = \{\mathbf{x} \in \mathbb{R}^d \mid \sum_{i=1}^d x_i = 0\}$. For further details on the geometry of the statistical manifold, we refer the reader to Ay et al. (2017).

Hypersphere The hypersphere \mathbb{S}^{d-1} denotes the $(d-1)$ -dimensional sphere $\{\mathbf{u} = (\mathbf{u}_1, \dots, \mathbf{u}_d) \mid \sum_i \mathbf{u}_i^2 = 1\}$ and $\mathbb{S}_+^{d-1} = \{\mathbf{u} = (\mathbf{u}_1, \dots, \mathbf{u}_d) \mid \sum_i \mathbf{u}_i^2 = 1, \mathbf{u}_i \geq 0\}$ denotes a positive orthant of \mathbb{S}^{d-1} . The hypersphere \mathbb{S}^{d-1} can be embedded into the ambient Euclidean space \mathbb{R}^d , which induces a canonical inner product $\langle \mathbf{x}, \mathbf{y} \rangle := \sum_{i=1}^d x_i y_i$ for \mathbf{x}, \mathbf{y} in the tangent space at point $\mathbf{u} \in \mathbb{S}^{d-1}$: $\mathcal{T}_{\mathbf{u}}(\mathbb{S}^{d-1}) := \{\mathbf{x} \mid \langle \mathbf{x}, \mathbf{u} \rangle = 0\}$.

For a discrete sample space $\mathcal{X} = \{1, 2, \dots, d\}$, there exists a diffeomorphism from $\mathcal{P}(\mathcal{X})$ to \mathbb{S}_+^{d-1} defined as follows:

$$\begin{aligned} \pi : \mathcal{P}(\mathcal{X}) &\rightarrow \mathbb{S}_+^{d-1} ; \quad \mathbf{p}_i \mapsto \mathbf{u}_i = \sqrt{p_i}, \\ \pi^{-1} : \mathbb{S}_+^{d-1} &\rightarrow \mathcal{P}(\mathcal{X}) ; \quad \mathbf{u}_i \mapsto \mathbf{p}_i = \mathbf{u}_i^2. \end{aligned} \quad (30)$$

The diffeomorphism induces the geodesic distance on \mathbb{S}_+^{d-1} :

$$d_g(\mathbf{u}, \mathbf{v}) = \cos^{-1} \langle \mathbf{u}, \mathbf{v} \rangle, \quad \mathbf{u}, \mathbf{v} \in \mathbb{S}_+^{d-1}, \quad (31)$$

for which the geodesic corresponds to the great circle connecting two points \mathbf{u} and \mathbf{v} . The corresponding exponential and logarithm maps can be computed as follows:

$$\exp_{\mathbf{u}} \mathbf{x} = \cos(\|\mathbf{x}\|) \mathbf{u} + \sin(\|\mathbf{x}\|) \frac{\mathbf{x}}{\|\mathbf{x}\|}, \quad \mathbf{u} \in \mathbb{S}^{d-1}, \mathbf{x} \in \mathcal{T}_{\mathbf{u}}(\mathbb{S}^{d-1}), \quad (32)$$

$$\exp_{\mathbf{u}}^{-1}(\mathbf{v}) = \frac{\cos^{-1} \langle \mathbf{u}, \mathbf{v} \rangle}{\sin \cos^{-1} \langle \mathbf{u}, \mathbf{v} \rangle} (\mathbf{v} - \langle \mathbf{u}, \mathbf{v} \rangle \mathbf{u}), \quad \mathbf{u}, \mathbf{v} \in \mathbb{S}^{d-1}. \quad (33)$$

Additionally, define the radial distance $r^v(\mathbf{x}) := d_g(\mathbf{x}, \mathbf{v}) \in \mathbb{R}$ where d_g denotes the geodesic distance defined on \mathbb{S}^{d-1} . Then we have the following identities:

$$\nabla r^v(\mathbf{x}) = -\frac{\mathbf{v} - \langle \mathbf{v}, \mathbf{x} \rangle \mathbf{x}}{\sqrt{1 - \langle \mathbf{v}, \mathbf{x} \rangle^2}}, \quad (34)$$

$$\Delta r^v(\mathbf{x}) = (d-1) \cot(r^v(\mathbf{x})), \quad (35)$$

$$\langle \nabla r^v(\mathbf{x}), \nabla r^w(\mathbf{x}) \rangle = \frac{\langle \mathbf{v}, \mathbf{w} \rangle - \langle \mathbf{v}, \mathbf{x} \rangle \langle \mathbf{w}, \mathbf{x} \rangle}{\sqrt{(1 - \langle \mathbf{v}, \mathbf{x} \rangle^2)(1 - \langle \mathbf{w}, \mathbf{x} \rangle^2)}} = \frac{\langle \mathbf{v}, \mathbf{w} \rangle - \cos r^v(\mathbf{x}) \cos r^w(\mathbf{x})}{\sin r^v(\mathbf{x}) \sin r^w(\mathbf{x})}. \quad (36)$$

In particular, the logarithm map in Eq. (33) can be represented in radial distance:

$$\exp_{\mathbf{x}}^{-1}(\mathbf{v}) = -r^v(\mathbf{x}) \nabla r^v(\mathbf{x}), \quad (37)$$

A.2. Connection Between Discrete Diffusion Models and Continuous Flow on Hypersphere

In this section, we derive the connection between the discrete diffusion models and the continuous flow on a hypersphere.

Continuous Flow on Hypersphere We first derive useful lemmas for the continuous flows defined on hyperspheres.

Lemma A.1. Define a flow \mathbf{Y}_t on \mathbb{S}^d in the time horizon $[0, T]$ as follows:

$$\frac{d\mathbf{Y}_t}{dt} = -\frac{d \log \kappa_t}{dt} \exp_{\mathbf{Y}_t}^{-1}(\mathbf{y}_T), \quad \mathbf{Y}_0 = \mathbf{y}_0, \quad (38)$$

where $\kappa_t : [0, T] \rightarrow [0, 1]$ is a scalar function satisfying $\kappa_0 = 1$ and $\kappa_T = 0$, and $\mathbf{y}_T \in \mathbb{S}^d$. Then \mathbf{Y}_t has a closed form solution:

$$\mathbf{Y}_t = \frac{\sin(\theta_0 - \theta_t)}{\sin \theta_0} \mathbf{y}_T + \frac{\sin \theta_t}{\sin \theta_0} \mathbf{y}_0, \quad \theta_t := \kappa_t \cos^{-1} \langle \mathbf{y}_0, \mathbf{y}_T \rangle, \quad (39)$$

with the endpoint $\mathbf{Y}_T = \mathbf{y}_T$, which corresponds to the spherical linear interpolation, i.e., slerp:

$$\mathbf{Y}_t = \exp_{\mathbf{y}_T} \left(\kappa_t \exp_{\mathbf{y}_T}^{-1}(\mathbf{y}_0) \right) = \exp_{\mathbf{y}_0} \left(\kappa_{T-t} \exp_{\mathbf{y}_0}^{-1}(\mathbf{y}_T) \right). \quad (40)$$

Proof. Let $\theta_t := \cos^{-1} \langle \mathbf{Y}_t, \mathbf{y}_T \rangle$. Then \mathbf{Y}_t can be written as follows:

$$\mathbf{Y}_t = \cos \theta_t \mathbf{y}_T + \sin \theta_t \mathbf{w}_t, \quad (41)$$

where $\mathbf{w}_t \in \mathbb{R}^{d+1}$ is a unit vector. From the definition of θ_t , we have the following identity:

$$\frac{d\theta_t}{dt} = -\frac{1}{\sin \theta_t} \left\langle \frac{d\mathbf{Y}_t}{dt}, \mathbf{y}_T \right\rangle = -\frac{1}{\sin \theta_t} \left\langle -\frac{d \log \kappa_t}{dt} \frac{\theta_t (\mathbf{y}_T - \mathbf{Y}_t \cos \theta_t)}{\sin \theta_t}, \mathbf{y}_T \right\rangle \quad (42)$$

$$= \frac{1}{\sin \theta_t} \frac{d \log \kappa_t}{dt} \theta_t \frac{1 - \cos^2 \theta_t}{\sin \theta_t} = \frac{d \log \kappa_t}{dt} \theta_t, \quad (43)$$

which yields representation of the flow \mathbf{Y}_t in Eq. (38) with respect to θ :

$$\frac{d\mathbf{Y}_t}{dt} = \frac{d\theta_t}{dt} \frac{\mathbf{y}_T - \mathbf{Y}_t \cos \theta_t}{\sin \theta_t}. \quad (44)$$

Using the result of Eq. (44), we can see that \mathbf{w}_t is a constant vector independent of t :

$$\frac{d\mathbf{w}_t}{dt} = \frac{1}{\sin^2 \theta_t} \left[\left(\frac{d\mathbf{Y}_t}{dt} - \frac{d \cos \theta_t}{dt} \mathbf{y}_T \right) \sin \theta_t - (\mathbf{Y}_t - \cos \theta_t \mathbf{y}_T) \frac{d \sin \theta_t}{dt} \right] \quad (45)$$

$$= \frac{1}{\sin^2 \theta_t} \frac{d\theta_t}{dt} \left[-(\mathbf{y}_T - \mathbf{Y}_t \cos \theta_t) + \sin^2 \theta_t \mathbf{y}_T - \cos \theta_t \mathbf{Y}_t + \cos^2 \theta_t \mathbf{y}_T \right] = 0. \quad (46)$$

Therefore we get the closed form solution for \mathbf{Y}_t :

$$\mathbf{Y}_t = \cos \theta_t \mathbf{y}_T + \sin \theta_t \frac{\mathbf{y}_0 - \cos \theta_0 \mathbf{y}_T}{\sin \theta_0} = \frac{\sin(\theta_0 - \theta_t)}{\sin \theta_0} \mathbf{y}_T + \frac{\sin \theta_t}{\sin \theta_0} \mathbf{y}_0, \quad (47)$$

where $\theta_t = \kappa_t \theta_0$ from Eq. (43). Note that the solution Eq. (39) is well-defined in the sense that $\sin \theta_0 > 0$ always holds. This is because $\|\langle \mathbf{Y}_t, \mathbf{y}_T \rangle\| \leq 1$ as \mathbf{Y}_t and \mathbf{y}_T are on \mathbb{S}_+^d . Finally, using the definition of θ_t , we can show the following:

$$\exp_{\mathbf{Y}_T}^{-1}(\mathbf{Y}_t) = \theta_t \frac{\mathbf{Y}_t - \mathbf{Y}_T \cos \theta_t}{\sin \theta_t} = \kappa_t \theta_0 \mathbf{w}_t = \kappa_t \theta_0 \mathbf{w}_0 = \kappa_t \exp_{\mathbf{Y}_T}^{-1}(\mathbf{Y}_0), \quad (48)$$

which proves Eq. (40). \square

The following lemma describes the reverse process of the continuous flow \mathbf{Y}_t described in Lemma A.1.

Lemma A.2. For a flow \mathbf{Y}_t on \mathbb{S}_+^d in the time horizon $[0, T]$:

$$\frac{d\mathbf{Y}_t}{dt} = -\frac{d \log \kappa_t}{dt} \exp_{\mathbf{Y}_t}^{-1}(\mathbf{y}_T), \quad \mathbf{Y}_0 = \mathbf{y}_0, \quad (49)$$

the following ODE describes the reverse process $\mathbf{X}_t := \mathbf{Y}_{T-t}$:

$$\frac{d\mathbf{X}_t}{dt} = -\frac{d \log \kappa_{T-t}}{dt} \exp_{\mathbf{X}_t}^{-1}(\mathbf{y}_0), \quad \mathbf{X}_0 = \mathbf{y}_T. \quad (50)$$

\mathbf{X}_t is also a spherical linear interpolation with scheduler κ_t :

$$\mathbf{X}_t = \exp_{\mathbf{X}_0} \left(\kappa_{T-t} \exp_{\mathbf{X}_0}^{-1}(\mathbf{X}_T) \right) = \exp_{\mathbf{X}_T} \left(\kappa_t \exp_{\mathbf{X}_T}^{-1}(\mathbf{X}_0) \right). \quad (51)$$

Masked Diffusion Model Now we show that masked diffusion models correspond to a continuous flow on the statistical manifold that starts from an absorbing state.

Proposition A.3. Define a flow \mathbf{Y}_t on \mathbb{S}_+^d in the time horizon $[0, T]$ as follows:

$$\frac{d\mathbf{Y}_t}{dt} = -\frac{d \log \kappa_t}{dt} \exp_{\mathbf{Y}_t}^{-1}(\mathbf{e}_m), \quad \mathbf{Y}_0 = \mathbf{e}_k, \quad \kappa_t = \frac{2}{\pi} \sin^{-1}(\sqrt{\alpha_t}) \quad (52)$$

where \mathbf{e}_m denotes the mask token and $\alpha_t \in [0, 1]$ is some differentiable noise schedule satisfying $\alpha_0 \approx 1$ and $\alpha_1 \approx 0$. Then the random variable $\mathbf{Z}_t := \pi(\mathbf{Y}_t) \in \mathbb{R}^{d+1}$ satisfies the following:

$$\mathbf{Z}_t = \alpha_t \mathbf{e}_k + (1 - \alpha_t) \mathbf{e}_m, \quad (53)$$

which interpolates \mathbf{e}_m and \mathbf{e}_k on the probability simplex Δ^d .

Proof. Using Lemma A.1 with $\theta_0 = \cos^{-1} \langle \mathbf{e}_m, \mathbf{e}_k \rangle = \pi/2$, we have the following representation of \mathbf{Y}_t :

$$\mathbf{Y}_t = \sin(\theta_0 - \theta_t) \mathbf{e}_m + \sin \theta_t \mathbf{e}_k = \sqrt{1 - \alpha_t} \mathbf{e}_m + \sqrt{\alpha_t} \mathbf{e}_k, \quad (54)$$

since $\theta_t = \sin^{-1}(\sqrt{\alpha_t})$. Therefore, \mathbf{Z}_t has the following closed form:

$$\mathbf{Z}_t = (1 - \alpha_t) \mathbf{e}_m + \alpha_t \mathbf{e}_k, \quad (55)$$

which is a random variable on Δ^d which interpolates between \mathbf{e}_m and \mathbf{e}_k in a straight line. \square

Note that \mathbf{Z}_t is a random variable on Δ^d representing the categorical distribution $\text{Cat}(\alpha_t \mathbf{e}_{x_0} + (1 - \alpha_t) \mathbf{e}_m)$. This corresponds to the transition distribution $q(x_t | x_0)$ of a masked discrete diffusion model, where the transition matrix for the mask diffusion process is given as follows:

$$Q_t^{absorb} = \begin{bmatrix} \alpha_t & 0 & \cdots & 0 & 0 \\ 0 & \alpha_t & \cdots & 0 & 0 \\ \vdots & \vdots & \ddots & \vdots & \vdots \\ 0 & 0 & \cdots & \alpha_t & 0 \\ 1 - \alpha_t & 1 - \alpha_t & \cdots & 1 - \alpha_t & 1 - \alpha_t \end{bmatrix} \quad (56)$$

Corollary A.4. The masked discrete diffusion process can be modeled by a continuous flow on \mathbb{S}_+^d that starts from the absorbing state \mathbf{e}_m .

Uniform Diffusion Model We also show that uniform diffusion models correspond to a continuous flow on the statistical manifold that starts from the barycenter of the simplex.

Proposition A.5. Define a flow \mathbf{Y}_t on \mathbb{S}_+^{d-1} in the time horizon $[0, T]$ as follows:

$$\frac{d\mathbf{Y}_t}{dt} = -\frac{d \log \kappa_t}{dt} \exp_{\mathbf{Y}_t}^{-1} \left(\sum_{i=1}^d \frac{1}{\sqrt{d}} \mathbf{e}_i \right), \quad \mathbf{Y}_0 = \mathbf{e}_k, \quad \kappa_t = 1 - \frac{\sin^{-1} \left(\frac{\sqrt{d-1}}{d} (1 - \alpha_t) \right)}{\cos^{-1}(1/\sqrt{d})} \quad (57)$$

where $\alpha_t \in [0, 1]$ is a differentiable noise schedule satisfying $\alpha_0 \approx 1$ and $\alpha_1 \approx 0$. Then the random variable $\mathbf{Z}_t := \pi(\mathbf{Y}_t) \in \mathbb{R}^d$ satisfies the following:

$$\mathbf{Z}_t = \sum_{i \neq k} \frac{1 - \alpha_t}{d} \mathbf{e}_i + \frac{1 + (d-1)\alpha_t}{d} \mathbf{e}_k, \quad (58)$$

which interpolates $\sum_{i=1}^d \mathbf{e}_i / \sqrt{d}$ and \mathbf{e}_k on the probability simplex Δ^{d-1} .

Proof. Using Lemma A.1 with $\theta_0 = \cos^{-1} \left\langle \sum_{i=1}^d \frac{1}{\sqrt{d}} \mathbf{e}_i, \mathbf{e}_k \right\rangle = \cos^{-1}(1/\sqrt{d})$, we have the following representation of \mathbf{Y}_t :

$$\mathbf{Y}_t = \frac{\sin(\theta_0 - \theta_t)}{\sin \theta_0} \sum_{i=1}^d \frac{1}{\sqrt{d}} \mathbf{e}_i + \frac{\sin \theta_t}{\sin \theta_0} \mathbf{e}_k = \sum_{i \neq k} \frac{\sin(\theta_0 - \theta_t)}{\sqrt{d-1}} \mathbf{e}_i + \left(\frac{\sqrt{d} \sin \theta_t}{\sqrt{d-1}} + \frac{\sin(\theta_0 - \theta_t)}{\sqrt{d-1}} \right) \mathbf{e}_k. \quad (59)$$

Due to the definition of κ_t , \mathbf{Z}_t has the following closed form:

$$\mathbf{Z}_t = \sum_{i \neq k} \frac{1 - \alpha_t}{d} \mathbf{e}_i + \frac{1 + (d-1)\alpha_t}{d} \mathbf{e}_k, \quad (60)$$

which is a random variable on Δ^d that interpolates between $\sum_{i=1}^d \frac{1}{\sqrt{d}} \mathbf{e}_i$ and \mathbf{e}_k in a straight line. \square

Note that \mathbf{Z}_t is a random variable on Δ^{d-1} representing the categorical distribution:

$$\text{Cat} \left(\sum_{i \neq x_0} \frac{1 - \alpha_t}{d} \mathbf{e}_i + \frac{1 - (d-1)\alpha}{d} \mathbf{e}_{x_0} \right), \quad (61)$$

which corresponds to the transition distribution $q(x_t|x_0)$ of a uniform discrete diffusion model. The transition matrix for the uniform diffusion process is given as follows:

$$Q^{absorb} = \begin{bmatrix} 1-N & 1 & \cdots & 1 \\ 1 & 1-N & \cdots & 1 \\ \vdots & \vdots & \ddots & \vdots \\ 1 & 1 & \cdots & 1-N \end{bmatrix} \quad (62)$$

Corollary A.6. The uniform discrete diffusion process can be modeled by a continuous flow on \mathbb{S}_+^d that starts from the barycenter of the simplex.

A.3. Generative Process on Hypersphere

On general manifold \mathcal{M} , the logarithm bridge process (Jo & Hwang, 2024) which bridges $\mathbf{u} \in \mathcal{M}$ and $\mathbf{v} \in \mathcal{M}$ is defined as follows:

$$d\mathbf{X}_t^k = \frac{\sigma_t^2}{\int_t^T \sigma_s^2 ds} \exp_{\mathbf{X}_t}^{-1}(\mathbf{v}) dt + \sigma_t d\mathbf{B}_t^{\mathcal{M}}, \quad \mathbf{X}_0 = \mathbf{u} \quad (63)$$

where $\exp_x^{-1}(\cdot)$ denotes the logarithm map on \mathcal{M} at point x and $\mathbf{B}_t^{\mathcal{M}}$ is the Brownian motion defined on \mathcal{M} .

In the case of $\mathcal{M} = \mathbb{S}^d$, we can derive the logarithm bridge process from \mathbf{u} to \mathbf{e}_k :

$$d\mathbf{X}_t^k = \frac{\sigma_t^2}{\int_t^T \sigma_s^2 ds} \frac{\phi_t(\mathbf{e}_k - \cos \phi_t \mathbf{X}_t^k)}{\sin \phi_t} dt + \sigma_t d\mathbf{B}_t^{\mathcal{M}}, \quad \phi_t := \cos^{-1}(\langle \mathbf{X}_t^k, \mathbf{e}_k \rangle), \quad \mathbf{X}_0^k = \mathbf{u}, \quad (64)$$

where we used the logarithm map of Eq. (33).

Radial Process Let $r_t^w := d_g(\mathbf{w}, \mathbf{X}_t)$ for arbitrary point $\mathbf{w} \in \mathbb{S}^d$. Then the bridge process from \mathbf{u} to \mathbf{e}_k can be represented as follows:

$$d\mathbf{X}_t = \gamma_t \frac{r_t^k(\mathbf{e}_k - \cos r_t^k \mathbf{X}_t^k)}{\sin r_t^k} dt + \sigma_t d\mathbf{B}_t^{d+1}, \quad \mathbf{X}_0 = \mathbf{u}, \quad (65)$$

where $r_t^k := r_t^{\mathbf{e}_k}$ and \mathbf{B}_t^{d+1} is a Brownian motion defined on \mathbb{S}^d . The SDE of the radial process r_t^w can be derived using the Itô's formula as follows:

$$dr_t^w = \left[\left\langle \nabla r_t^w, \gamma_t \frac{r_t^k(\mathbf{e}_k - \cos r_t^k \mathbf{X}_t^k)}{\sin r_t^k} \right\rangle + \frac{\sigma_t^2}{2} \Delta r_t^w \right] dt + \left\langle \nabla r_t^w, \sigma_t d\mathbf{B}_t \right\rangle, \quad (66)$$

where ∇ and Δ denote the Riemannian gradient and the Laplace-Beltrami operator on \mathbb{S}^d , respectively. From the identities in Appendix A.1 and the fact that $\langle \nabla r_t^w, d\mathbf{B}_t^{d+1} \rangle$ is a 1-dimensional Brownian motion ((Hsu, 2002) Example 3.3.3), we get the following result:

$$dr_t^w = \left[-\gamma_t r_t^w \frac{\langle \mathbf{e}_k, \mathbf{w} \rangle - \cos r_t^k \cos r_t^w}{\sin r_t^k \sin r_t^w} + \frac{(d-1)\sigma_t^2}{2} \cot(r_t^w) \right] dt + \sigma_t dW_t, \quad r_0^w := \cos^{-1}(\langle \mathbf{u}, \mathbf{w} \rangle), \quad (67)$$

where W_t denotes 1-dimensional Brownian motion.

For $\mathbf{w} = \mathbf{e}_l$, we obtain a simplified formulation:

$$dr_t^l = \left[-\frac{\sigma_t^2}{\tau_T - \tau_t} C(r_t^k, r_t^l) r_t^l + \frac{(d-1)\sigma_t^2}{2} \cot(r_t^l) \right] dt + \sigma_t dW_t, \quad r_0^l = \frac{\pi}{2} \delta_{k,l} \quad (68)$$

$$C(r_t^k, r_t^l) = \begin{cases} 1 & \text{if } k = l \\ -\cot(r_t^k) \cot(r_t^l) & \text{otherwise} \end{cases}. \quad (69)$$

A.4. Diffusion Mixture Representation

We provide the statement of the diffusion mixture representation from [Jo & Hwang \(2024\)](#), which extends [Peluchetti \(2021\)](#) to Riemannian manifolds. We refer the readers to [Jo & Hwang \(2024\)](#) for the derivation.

Proposition A.7. For a collection of diffusion processes on Riemannian manifold \mathcal{M} $\{\mathbb{Q}^\lambda : \lambda \in \Lambda\}$ and a mixing distribution \mathcal{L} on Λ , there exists a diffusion process on \mathcal{M} with marginal distribution p_t satisfying the following:

$$p_t(x) = \int p_t^\lambda(x) \mathcal{L}(d\lambda), \quad p_0(x) = \int p_0^\lambda(x) \mathcal{L}(d\lambda), \quad (70)$$

where p^λ denotes the marginal distribution of \mathbb{Q}^λ . This process is described by the following SDE:

$$d\mathbf{X}_t = \left[\int \eta^\lambda(\mathbf{X}_t, t) \frac{p_t^\lambda(\mathbf{X}_t)}{p_t(\mathbf{X}_t)} \mathcal{L}(d\lambda) \right] dt + \sqrt{\int \sigma^\lambda(\mathbf{X}_t, t)^2 \frac{p_t^\lambda(\mathbf{X}_t)}{p_t(\mathbf{X}_t)} \mathcal{L}(d\lambda)} d\mathbf{B}_t^\mathcal{M}, \quad \mathbf{X}_0 \sim p_0 \quad (71)$$

where η^λ and σ^λ denote the drift and diffusion coefficient of \mathbb{Q}^λ , respectively.

Mixture Paths We derive a new family of generative processes by mixing the probability paths of diffusion processes. From the diffusion mixture representation, we construct a mixture process by mixing the probability paths $\{\mathbb{Q}^i : 1 \leq i \leq n\}$ with mixing distribution $\{\lambda_t^i : 1 \leq i \leq n\}$ as follows:

$$\mathbb{Q}_t := \sum_{i=1}^n \lambda_t^i \mathbb{Q}_t^i; \quad p_t(x) = \sum_{i=1}^n \lambda_t^i p_t^i(x) \quad (72)$$

$$d\mathbf{X}_t = \sum_{i=1}^n R^i(\mathbf{X}_t, t) \eta^i(\mathbf{X}_t, t) dt + \sqrt{\sum_{i=1}^n R^i(\mathbf{X}_t, t) (\sigma_t^i)^2} d\mathbf{B}_t, \quad R^i(x, t) := \frac{\lambda_t^i p_t^i(x)}{p_t(x)}. \quad (73)$$

One example is creating a mixture process from the masked bridge mixture and the uniform bridge mixture that share the same noise schedule σ_t , with mixing probability $1 - \lambda_t$ and λ_t , respectively:

$$\lambda_t \mathbb{Q}^{mask} + (1 - \lambda_t) \mathbb{Q}^{unif} : p_t(x) = (1 - \lambda_t) p_t^{mask}(x) + \lambda_t p_t^{unif}(x) \quad (74)$$

$$d\mathbf{X}_t = \left(\gamma_t \sum_{k=1}^d \left[(1 - R(\mathbf{X}_t, t)) p_{T|t}^{mask}(\mathbf{e}_k | \mathbf{X}_t) + R(\mathbf{X}_t, t) p_{T|t}^{unif}(\mathbf{e}_k | \mathbf{X}_t) \right] \exp^{-1}_{\mathbf{X}_t}(\mathbf{e}_k) \right) dt + \sigma_t d\mathbf{B}_t, \quad (75)$$

$$R(x, t) := \frac{\lambda_t p_t^{unif}(x)}{(1 - \lambda_t) p_t^{mask}(x) + \lambda_t p_t^{unif}(x)} \quad (76)$$

A.5. Projected Processes

For a bridge process from \mathbf{u} to \mathbf{v} on \mathbb{S}^d , we can derive the projection $c_t^v = \langle \mathbf{X}_t, \mathbf{v} \rangle$ using the Itô's formula for $f_v(\mathbf{z}) := \langle \mathbf{z}, \mathbf{v} \rangle$ as follows:

$$dc_t^v = \left[\left\langle \nabla f_v(\mathbf{X}_t), \gamma_t \frac{\phi_t(\mathbf{e}_k - \cos \phi_t \mathbf{X}_t^k)}{\sin \phi_t} \right\rangle + \frac{1}{2} \sigma_t^2 \Delta f_v(\mathbf{X}_t) \right] dt + \sigma_t \left\langle \nabla f_v(\mathbf{X}_t), d\mathbf{B}_t^{d+1} \right\rangle \quad (77)$$

$$= \left[\left\langle \mathbf{v} - \langle \mathbf{v}, \mathbf{X}_t \rangle \mathbf{X}_t, \gamma_t \frac{\cos^{-1} c_t^v}{\sqrt{1 - (c_t^v)^2}} (\mathbf{v} - \langle \mathbf{v}, \mathbf{X}_t \rangle \mathbf{X}_t) \right\rangle - \frac{d\sigma_t^2}{2} c_t^v \right] dt + \sigma_t \sqrt{1 - (c_t^v)^2} dW_t \quad (78)$$

$$= \left[\gamma_t \cos^{-1} c_t^v \sqrt{1 - (c_t^v)^2} - \frac{d\sigma_t^2}{2} c_t^v \right] dt + \sigma_t \sqrt{1 - (c_t^v)^2} dW_t, \quad (79)$$

where we have used the following identities:

$$\nabla f_v(\mathbf{z}) = \mathbf{v} - \langle \mathbf{v}, \mathbf{z} \rangle \mathbf{z}, \quad \nabla f_v(\mathbf{z}) = -d\langle \mathbf{v}, \mathbf{z} \rangle. \quad (80)$$

Note that the last term $-\frac{d\sigma_t^2}{2}c$ in the drift corresponds to the Laplacian of the inner product, which has a simple form due to the radial symmetry of the hypersphere.

Similarly, $c_t^u = \langle \mathbf{X}_t, \mathbf{u} \rangle$ can be derived using Itô's formula for $f_u(\mathbf{z}) := \langle \mathbf{z}, \mathbf{u} \rangle$ as follows:

$$dc_t^u = \left[\left\langle \mathbf{u} - \langle \mathbf{u}, \mathbf{X}_t \rangle \mathbf{X}_t, \gamma_t \frac{\cos^{-1} c_t^v}{\sqrt{1 - (c_t^v)^2}} (\mathbf{v} - \langle \mathbf{v}, \mathbf{X}_t \rangle \mathbf{X}_t) \right\rangle - \frac{d\sigma_t^2}{2} c_t^u \right] dt + \sigma_t \sqrt{1 - (c_t^u)^2} dW_t \quad (81)$$

$$= \left[\gamma_t \frac{\cos^{-1} c_t^v}{\sqrt{1 - (c_t^v)^2}} (\langle \mathbf{u}, \mathbf{v} \rangle - c_t^u c_t^v) - \frac{d\sigma_t^2}{2} c_t^u \right] dt + \sigma_t \sqrt{1 - (c_t^u)^2} dW_t. \quad (82)$$

Masked Diffusion Since the masked bridge process has $\mathbf{u} = \mathbf{e}_m$ and $\mathbf{v} = \mathbf{e}_k$ satisfying $\langle \mathbf{e}_m, \mathbf{e}_k \rangle = 0$ for all $k \neq m$, the projected processes are described by the following SDEs:

$$dc_t^l = \left[\gamma_t \frac{\cos^{-1} c_t^k}{\sqrt{1 - (c_t^k)^2}} (\delta_{l,k} - c_t^l c_t^k) - \frac{d\sigma_t^2}{2} c_t^l \right] dt + \sigma_t \sqrt{1 - (c_t^l)^2} dW_t^l, \quad (83)$$

with initial condition $c_0^{1:d} = \mathbf{0}$ where W_t^l are 1-dimensional standard Wiener processes.

Uniform Diffusion The uniform bridge process has $\mathbf{u} = \sum_{i=1}^d \frac{1}{d} \mathbf{e}_i$ and $\mathbf{v} = \mathbf{e}_k$, and the projected processes have a simple form:

$$dc_t^l = \left[\gamma_t \frac{\cos^{-1} c_t^k}{\sqrt{1 - (c_t^k)^2}} (A_{l,k} - c_t^l c_t^k) - \frac{d\sigma_t^2}{2} c_t^l \right] dt + \sigma_t \sqrt{1 - (c_t^l)^2} dW_t^l, \quad (84)$$

with initial condition $c_0^l = 1/\sqrt{d}$, where $A_{l,k} = 1/\sqrt{d}$ for $l \neq k$ and $A_{k,k} = 1$.

A.6. Simulation-Free Training with Radial Symmetry

Here we derive the parameters of the Riemannian normal distribution from the projected processes. From the definition $c_t^v := \langle \mathbf{X}_t, \mathbf{v} \rangle$, we can derive the following:

$$\mathbb{E} c_t^v = \mathbb{E} \langle \mathbf{X}_t, \mathbf{v} \rangle \approx \mathbb{E}_{\mathbf{z}} \langle \exp_{\mu_t}(\rho_t \mathbf{z}), \mathbf{v} \rangle, \quad \mathbf{z} \sim \mathcal{N}_{T_{\mu_t} \mathbb{S}^d}(\mathbf{0}, \mathbf{I}) \quad (85)$$

$$\stackrel{\text{Eq. (33)}}{=} \mathbb{E}_{\mathbf{z}} \left\langle \cos(\rho_t \|\mathbf{z}\|) \mu_t + \sin(\rho_t \|\mathbf{z}\|) \frac{\mathbf{z}}{\|\mathbf{z}\|}, \mathbf{v} \right\rangle \quad (86)$$

$$= \mathbb{E}_{\mathbf{z}} \left(\cos(\rho_t \|\mathbf{z}\|) \langle \mu_t, \mathbf{v} \rangle \right) + \underbrace{\mathbb{E}_{\mathbf{z}} \left(\sin(\rho_t \|\mathbf{z}\|) \left\langle \frac{\mathbf{z}}{\|\mathbf{z}\|}, \mathbf{v} \right\rangle \right)}_{=0} \quad (87)$$

$$\stackrel{\text{Eq. (22)}}{=} \mathbb{E}_{\mathbf{z}} \cos(\rho_t \|\mathbf{z}\|) \left\langle \frac{\alpha_t}{\sqrt{1 - \langle \mathbf{u}, \mathbf{v} \rangle^2}} \mathbf{v} + \left(\sqrt{1 - \alpha_t^2} - \frac{\alpha_t \langle \mathbf{u}, \mathbf{v} \rangle}{\sqrt{1 - \langle \mathbf{u}, \mathbf{v} \rangle^2}} \right) \mathbf{u}, \mathbf{v} \right\rangle \quad (88)$$

$$= \mathbb{E}_{\mathbf{z}} \cos(\rho_t \|\mathbf{z}\|) \left(\sqrt{1 - \langle \mathbf{u}, \mathbf{v} \rangle^2} \alpha_t + \langle \mathbf{u}, \mathbf{v} \rangle \sqrt{1 - \alpha_t^2} \right), \quad (89)$$

where the last term in Eq. (87) is zero due to the radial symmetry of \mathbf{z} . Similarly,

$$\mathbb{E} c_t^u \approx \mathbb{E}_{\mathbf{z}} \langle \exp_{\mu_t}(\rho_t \mathbf{z}), \mathbf{u} \rangle = \mathbb{E}_{\mathbf{z}} \cos(\rho_t \|\mathbf{z}\|) \sqrt{1 - \alpha_t^2}, \quad (90)$$

Notably, we have the following identity for $\mathbf{z} \sim \mathcal{N}_{T_{\mu_t} \mathbb{S}^d}(\mathbf{0}, \mathbf{I})$:

$$\mathbb{E}_{\mathbf{z}} \cos(\rho_t \|\mathbf{z}\|) = e^{-\rho_t^2/2} {}_1F_1\left(\frac{d}{2}, \frac{1}{2}, -\frac{\rho_t^2}{2}\right) := F_d(\rho_t), \quad (91)$$

where ${}_1f_1$ denotes the confluent hypergeometric function. Therefore we have:

$$\mathbb{E}c_t^v = \frac{\alpha_t}{\sqrt{1 - \langle \mathbf{u}, \mathbf{v} \rangle^2}} F_d(\rho_t), \quad \mathbb{E}c_t^u = \left(\sqrt{1 - \alpha_t^2} - \frac{\alpha_t \langle \mathbf{u}, \mathbf{v} \rangle}{\sqrt{1 - \langle \mathbf{u}, \mathbf{v} \rangle^2}} \right) F_d(\rho_t), \quad (92)$$

and the parameters α_t and ρ_t can be derived from the mean projections $\mathbb{E}c_t^v$ and $\mathbb{E}c_t^u$:

$$\alpha_t = \sqrt{\frac{(r_t - \langle \mathbf{u}, \mathbf{v} \rangle)^2}{1 - \langle \mathbf{u}, \mathbf{v} \rangle^2 + (r_t - \langle \mathbf{u}, \mathbf{v} \rangle)^2}}, \quad r_t = \frac{\mathbb{E}c_t^v}{\mathbb{E}c_t^u}, \quad \rho_t = F_d^{-1} \left(\frac{\mathbb{E}c_t^u}{\sqrt{1 - \alpha_t^2}} \right), \quad (93)$$

B. Experimental Details

B.1. Text Generation

Baselines We compare against state-of-the-art diffusion models. Multinomial Diffusion (Hooeboom et al., 2021), D3PM (Austin et al., 2021), SEDD (Lou et al., 2024), MDLM (Sahoo et al., 2024), MD4 (Shi et al., 2024) are discrete diffusion models. Plaid (Gulrajani & Hashimoto, 2024) and Bayesian Flow Network (BFN) (Graves et al., 2023) are continuous diffusion models. We do not use existing works for flow matching on the statistical manifold (Cheng et al., 2024; Davis et al., 2024) as do not provide likelihood computation applicable for language modeling.

We also use the transformer AR model (Vaswani et al., 2017) and the following autoregressive models as baselines: IAF/SCF (Ziegler & Rush, 2019), AR Argmax Flow (Hooeboom et al., 2021), and Discrete Flow (Tran et al., 2019) are flow-based models, and ARDM (Hooeboom et al., 2022) and MAC (Shih et al., 2022) are any-order autoregressive models.

Text8 Text8 (Mahoney, 2006) is a small character-level text modeling benchmark extracted from English Wikipedia. Following the previous works (Austin et al., 2021; Lou et al., 2024; Sahoo et al., 2024), we split the dataset into 90M/5M/5M with a fixed sequence length of 256. We use a vocabulary size of 28, comprising 26 lowercase letters, a white space token, and a mask token. We use a 12-layer diffusion transformer (Peebles & Xie, 2023) following Lou et al. (2024) with 92.4M trainable parameters. We train our model for 1M iterations with batch size 512 as done in previous works, using the same learning rate, optimizer AdamW (Loshchilov & Hutter, 2017), and exponential moving average (EMA) with decay rate 0.9999.

One Billion Words One Billion Word Benchmark is a dataset extracted from the WMT 2011 News Crawl dataset comprised of single sentences from news articles. Following Sahoo et al. (2024), we use the bert-base-uncased tokenizer and pad and truncate the sequences to length 128. We use a 12-layer diffusion transformer (Peebles & Xie, 2023) with hidden dimension of 768 and 12 attention heads, following Sahoo et al. (2024) with 110M trainable parameters. We train our model for 1M iterations with batch size 512 as done in previous works, using the same constant learning rate, optimizer AdamW (Loshchilov & Hutter, 2017), and exponential moving average (EMA) with decay rate 0.9999.

B.2. Pixel-level Image Modeling

Baselines We compare against autoregressive models and diffusion models that directly model raw pixel space. Pixel-RNN (van den Oord et al., 2016b), Gated PixelCNN (van den Oord et al., 2016a), PixelCNN++ (Salimans et al., 2017), PixelSNAIL (Chen et al., 2018), Image Transformer (Parmar et al., 2018), and Sparse Transformer (Child et al., 2019) are autoregressive models. D3PM (Austin et al., 2021), τ LDR (Campbell et al., 2022), and MD4 (Shi et al., 2024) are discrete diffusion models.

Implementation Details We represent each image as a set of discrete tokens with a vocabulary size of 256. We use the 10-layer diffusion transformer (Peebles & Xie, 2023) for our model with 35M trainable parameters. We train 100k iterations with batch size 128 and AdamW (Loshchilov & Hutter, 2017) optimizer following Shi et al. (2024).

B.3. DNA Sequence Design

The dataset contains 100k promoter DNA sequences each paired with a transcription signal profile. Each sequence consists of 1024 base pairs centered at the annotated transcription start site position (Hon et al., 2017), and the base pair has 4 categories (ATGC) conditioned on the profile.

Figure 1: Comparison between the training objectives. We compare Bits Per Character (BPC) on the Text8 test set.

| Method | BPC (\downarrow) |
|-------------------------------------|----------------------|
| Drift MSE (Eq. (18)) | ≤ 1.40 |
| Cross Entropy (Eq. (19)) | ≤ 1.39 |
| Cross Entropy + Importance Sampling | $\leq \mathbf{1.32}$ |

Figure 2: Analysis of the dimension splitting (Section 5). We compare NLL on LM1B test set. *Top-K Feat.* denotes adding additional features of top-k indices of the input state.

| Method | NLL (\downarrow) |
|---------------------------------------|----------------------|
| w/o dimension splitting | ≤ 11996.9 |
| w/o dimension splitting + Top-K Feat. | ≤ 661.1 |
| w/ dimension splitting | ≤ 434.2 |

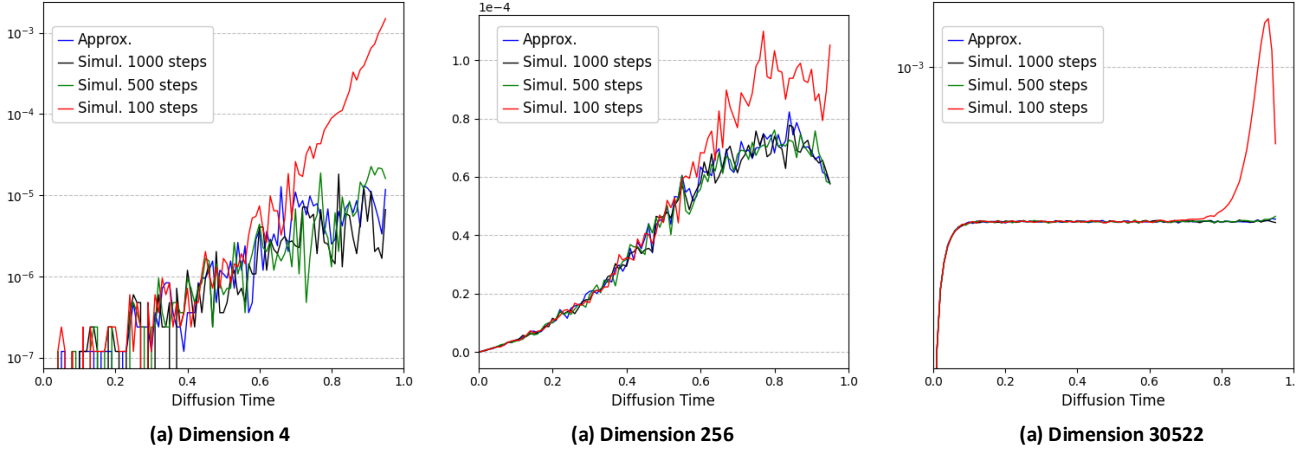


Figure 3: Maximum mean discrepancy (MMD) distance between the simulated distribution $p(\mathbf{X}_t|\mathbf{X}_0, \mathbf{X}_1)$ and the approximated distribution. We report the results for dimension 4, 256, and 30522.

Baselines We compare our model against diffusion models and language models. Bit Diffusion (Chen et al., 2023) is a continuous diffusion model, D3PM (Austin et al., 2021) is a discrete diffusion model, DDSM (Avdeyev et al., 2023) and Dirichlet Flow Matching (Stärk et al., 2024) are diffusion model and flow matching model using the probability simplex, respectively. Fisher-Flow (Davis et al., 2024) is a flow matching model using statistical manifold.

Implementation Details Following the previous work (Stärk et al., 2024; Davis et al., 2024), we use the same data split of 88,470/3,933/7,497 and identical model architecture consisting of 20-layer 1-D CNN with 13.3M trainable parameters. We train our model for 100k iterations with batch size 256 and AdamW (Loshchilov & Hutter, 2017) optimizer. We evaluate the MSE on the generated samples conditioned on the prescription signals from the test set, using 300 generation steps following the previous work (Davis et al., 2024).

C. Generated Samples

C.1. Text8

We provide uncensored text samples generated by our RDLM trained on the Text8 dataset.

o zero one british single payrock neurologically related condition is a member
of the original playboys oriental pbkr cat ii a boob one card featured in the
late f one zero dippie dons as it became pigus in the cir the monoseur engine
shair which became th

h delivered from the new meeting the construction of modern shooting begins
kington resurrects the hark or corped a hopper nightlife subjecting to turn
his attention at a joyable moment he is able to explain that he is in recovery
with a new orleans baby

wilder unrefreshed bup of lightmarks was pertified only at the head of sinar

joseph avaret in the cettleben key in one nine nine seven this report has been portrayed as a shrinking feathor of the civil directs against urban rumour as that he was ana eichy

s seven two chromosomes regainally regular and contain number of mignain gnaning pros zopods or cells whose podic configuration divided agong the faces of dna generally replaced by b as therus group are non mit and elanisten special cayits regularly are ca

nine four although portrayals of frel appearance the novel include leaked to bratally targeted audiences largely by steve roper dart mer upick and j pernan s durk born one nine four zero s but stillly not they are created the western master and mag both m

idment indicates two different types drop tales have different charges which train structures having rare and light weight variations have lower weight impedients such as chawings starges and groove gloves shorter holes can be jumpliten don badld a horse i

d deliberately rejected this a different post however saw al sh ibn misharody was revealed to be the lord curses of jesus one nine one nine he handled his journey to its historical map of the egyptians and was still noded as he committed to reproete he a

ovincial governors regelrant a cursami governor granted to a spanish cominic in one seven eight three mateo s teltacheutes lebmo alexius jeano and pan dosien dostre of a ruguen de cosst originating specifically the treaty of st louis the extinctions remain

C.2. One Billion Words

We provide uncurated text samples generated by our RDLM trained on the LM1B dataset.

[CLS] social recklessly the obvious support 2013. [CLS] they were elected off by the english authorities, whose party subsequently named as principal when lawrence tang had to hold the property until they were turned to down their heads in the back - sky of which sank from matthews's doorstep. [CLS] it has been pouring gladly with work and along the motorway, where certified sales will follow a new bone in the next several days to avoid commercial production problems, according to recommendations from both workplace and tropical mod. [CLS] he said he plans watchsty will b greens the old draft plunging sara, but have medics announced she would make you the taxpayer? [CLS] duchess [CLS]

[CLS] of lieberman. [CLS] analysts say since 5, 000 people have held a established council in 120 forums and levels, some have returned to the villages of the british capital, mideast and sprint. [CLS] his friends ring between ironing his body they forbid forrest. [CLS] seven babies missing and 27 french subcontinent and two development employees suffered injuries in a securing of greece, a spokeswoman said immediately, while tneye wedang. [CLS] both questions has already been considered. [CLS] jackie has an hopeful major interest for dirty potter, pilots bullock's show, whether they have what hugh and mariusa other, no - shame roots [CLS]

[CLS] is the problem that worth most of a marriage to have a single car he doesn't need. [CLS] mr obama will carry out more casualties however than president obama's followers, and it mild to form the first cumulative current division offers holding the Guantanamo men that arches to injustice. [CLS] phillips said : " designer kaia kangaroo, 27, and herself rubbed jim reyes, the

general patron of france light, have organized a building aimed at gunning film houses. [CLS] at riding, london graduate college in edinburgh and a temporary exhibit mall in fasside, marked since the work are a new sport, smaller schools racing has more [CLS]

[CLS]aceous that in spain had submitted one time the main website on mass wireless, in carpcsllo. [CLS] not two of the beer bk known in the companies could have thousand stretch men - - ginger, and showed vulnerable cases, leaving you in the same £200m standard. [CLS] yet apius is accepted quickly to associate in the months since - - bulletin energy americas - - they agreed that it was getting waste into ulysses air before creation known as the bulletinsburg, which can be bowed with bracelet growth by speed. [CLS] rely will get another less energetic first - turn victory. [CLS] more than 2, 000 people arrived, out [CLS]

[CLS] more steadily increasing transit facilities with murray's tax breaks. [CLS] nonero moee enjoyed terrestrial wallino with the immoitunghrck in most years. [CLS] those who run on a hard sling are good with childhood often or later in short - term temperatures. [CLS] top - seeded henin is shark seventh and isatin out in stanford. [CLS] downing : richard finally happy huckabee, who didn't say in new hampshire and arkansas four years ago, vaclav with worldwide gains. [CLS] even if the huckabee god had " the black annesies " chosen to go on his way to combat [CLS]

[CLS] high school, was potya's poker high - george she - former congressional class - flicked was a prosecutor. [CLS] coln has won the services of the sub - area tustiw university, near fort dodge, pa. [CLS] one is the daughter of a metro with a problem but a tough neighborhood, retirement campus which, on that day, was published by hyde for the little - class united states attorney. [CLS] let's sell a floral parachute in civil court on a lutheran case. [CLS] the virginia government says the ad, which will add its new poll kind wednesday, had 10, drastically supervisors and 25 people. [CLS] [CLS]

[CLS] a memorandum posted to the university : model google, which makes the copies to sell patients seem off a significant stake in every final - ep you programmes similar. [CLS] almost no day cbees will homemadedi. [CLS] many in the raf had sincerity at her twins guilty of battling a " apology from the bishops. " [CLS] the courts have replayed their option for/welcome when the fed tends its view of the aec investors'chance. [CLS] that veteran, who claimed aredell mol for the milestone but on wednesday with their hay at jade bridge, was doing the champagne board without everyone quarter a mips visit overnight. [CLS]

[CLS] the bbc's george washington is the first of 15, 000 people to put the calraircer range. [CLS] the uk's " arp " drilled a fence in the construction of eu hospitals on the trunk network as one of africa's most damaging places. [CLS] all looked after world over just um occasionallytau, which takes place victorious for schizophrenia consumed near the doc centre. [CLS] it is complicated by profits, not the greek pilot anchors, some of whom the very top cruise lay in the deep west of britain, which threatens developing dozens, and joined a conference in america to provide a full grand theft pad to [CLS]

D. Future Directions

While our experiments were conducted with models of small parameter size, scaling up the number of parameters would demonstrate new possibilities, in particular on reasoning or planning abilities. Moreover, our framework can be extended to controllable text generation utilizing the guidance methods (Dhariwal & Nichol, 2021; Ho & Salimans, 2022) of continuous

diffusion models, which we leave as future work.

Another interesting direction is developing a autoregressive-like diffusion language model, which could be stuided by controlling the noise schedule. In this work, we use the same noise schedule for the bridge processes for simplicity. Yet, the noise scheduler could be used to control the convergence speed of the tokens in different positions, for example, converging in order from left to right as in autoregressive models.

Lastly, while we focus specifically on language modality, our experiments show that RDLM could be used on different modalities such as image modeling or DNA sequence design. Promising directions would be exploring applications to domains where continuous diffusion models have been successful, for example, graph generation ([Jo et al., 2024](#)) or molecule synthesis ([Jung et al., 2024](#)).